



1 **Simulating Lightning NO<sub>x</sub> Production in CMAQv5.2 Using mNLDN, hNLDN,**  
2 **and pNLDN Schemes: Performance Evaluations**

3

4 Daiwen Kang<sup>1\*</sup>, Kristen Foley<sup>1</sup>, Rohit Mathur<sup>1</sup>, Shawn Roselle<sup>1</sup>, Kenneth Pickering<sup>2</sup>, and Dale  
5 Allen<sup>2</sup>

6

7 <sup>1</sup>Computational Exposure Division, National Exposure Research Laboratory, U.S.

8 Environmental Protection Agency, Research Triangle Park, NC 27711, USA

9 <sup>2</sup>Department of Atmospheric and Oceanic Science, University of Maryland, College Park, MD,

10 USA

11

12

13

14

15

16

17

18

19

20

21

22

23 \*Corresponding author: Daiwen Kang, US EPA, 109 T.W. Alexander Drive, Research Triangle Park, NC

24 27711, USA. Tel.: 919-541-4587; fax: 919-541-1379; e-mail: kang.daiwen@epa.gov



25

## Abstract

26 This study assesses the impact of the lightning  $\text{NO}_x$  ( $\text{LNO}_x$ ) production schemes in the  
27 CMAQ model (Kang et al., 2019) on ground-level air quality as well as aloft atmospheric  
28 chemistry through detailed evaluation of model predictions of nitrogen oxides ( $\text{NO}_x$ ) and ozone  
29 ( $\text{O}_3$ ) with corresponding observations for the U.S. For ground-level evaluations, hourly  $\text{O}_3$  and  
30  $\text{NO}_x$  from the US EPA's AQS monitoring network are used to assess the impact of different  
31  $\text{LNO}_x$  schemes on model prediction of these species in time and space. Vertical evaluations are  
32 performed using ozonesonde and P-3B aircraft measurements during the DISCOVER-AQ  
33 campaign conducted in the Baltimore/Washington region during July 2011. The impact on wet  
34 deposition of nitrate is assessed using measurements from the National Atmospheric Deposition  
35 Program's National Trends Network (NADP/NTN). Compared with the base model (without  
36  $\text{LNO}_x$ ), the impact of  $\text{LNO}_x$  on surface  $\text{O}_3$  varies from region to region depending on the base  
37 model conditions. Overall statistics suggest that for regions where surface  $\text{O}_3$  mixing ratios are  
38 already overestimated, the incorporation of additional  $\text{NO}_x$  from lightning generally increased  
39 model overestimation of mean daily maximum 8-hr (DM8HR)  $\text{O}_3$  by 1-2 ppb. In regions where  
40 surface  $\text{O}_3$  is underestimated by the base model,  $\text{LNO}_x$  can significantly reduce the  
41 underestimation and bring model predictions close to observations. Analysis of vertical profiles  
42 reveals that  $\text{LNO}_x$  can significantly improve the vertical structure of modeled  $\text{O}_3$  distributions by  
43 reducing underestimation aloft, and to a lesser degree decreasing overestimation near the surface.  
44 Since the base model underestimates the wet deposition of nitrate in most regions across the  
45 modeling domain except the Pacific Coast, the inclusion of  $\text{LNO}_x$  leads to reduction in biases  
46 and errors and an increase in correlation coefficients at almost all the NADP/NTN sites. Among  
47 the three  $\text{LNO}_x$  schemes described in Kang et al. (2019), the hNLDN scheme, which is  
48 implemented using hourly observed lightning flash data from National Lightning Detection  
49 Network (NLDN), performs best for the ground-level, vertical profiles, and wet deposition  
50 comparisons except that for the accumulated wet deposition of nitrate, the mNLDN scheme (the  
51 monthly NLDN-based scheme) performed slightly better. However, when observed lightning  
52 flash data are not available, the linear regression-based parameterization scheme, pNLDN,  
53 provides an improved estimate for  $\text{LNO}_x$  compared to the base simulation that does not include  
54  $\text{LNO}_x$ .



## 55 1. Introduction

56 The potential importance of NO<sub>x</sub> produced by lightning (LNO<sub>x</sub>) on regional air quality was  
57 recognized more than two decades ago (e.g. Novak and Pierce, 1993), but LNO<sub>x</sub> emissions have  
58 only been added to regional chemistry and transport models during the last decade (e.g. Allen et  
59 al., 2012; Kaynak et al., 2008; Koshak et al., 2014; Smith and Mueller, 2010; Koo et al., 2010)  
60 owing in part to the limited understanding of this NO<sub>x</sub> source (Schumann and Huntrieser, 2007;  
61 Murray, 2016; Pickering et al., 2016). As a result of efforts to reduce anthropogenic NO<sub>x</sub>  
62 emissions in recent decades (Simon et al., 2015; <https://gispub.epa.gov/air/trendsreport/2018>), it  
63 is expected that the relative contribution of LNO<sub>x</sub> to the tropospheric NO<sub>x</sub> burden and its  
64 subsequent impacts on atmospheric chemistry will increase in the United States and other  
65 developed countries (Kang and Pickering, 2018). The significant impact of LNO<sub>x</sub> on surface air  
66 quality was earlier reported by Napelenok et al. (2008), in that low-biases in upper tropospheric  
67 NO<sub>x</sub> in Community Multiscale Air Quality Model (CMAQ) (Byun and Schere, 2006)  
68 simulations without LNO<sub>x</sub> emissions made it difficult to constrain ground-level NO<sub>x</sub> emissions  
69 using inverse methods and Scanning Imaging Absorption Spectrometer for Atmospheric  
70 Cartography (SCIAMACHY) NO<sub>2</sub> retrievals (Bovensmann et al., 1999; Sioris et al., 2004;  
71 Richter et al., 2005). Appel et al. (2011) and Allen et al. (2012) reported that NO<sub>3</sub><sup>-</sup> wet deposition  
72 at National Atmospheric Deposition Program (NADP) sites was underestimated by a factor of  
73 two when LNO<sub>x</sub> was not included.

74 LNO<sub>x</sub> production and distribution were parameterized initially in global models (e.g.  
75 Stockwell et al., 1999; Labrador et al., 2005) relying on the work of Price and Rind (1992) and  
76 Price et al. (1997) in that lightning flash frequency was parameterized as a function of the  
77 maximum cloud-top-height. Other approaches for LNO<sub>x</sub> parameterization include a combination  
78 of latent heat release and cloud-top-height (Flatoy and Hov, 1997), convective precipitation rate  
79 (e.g. Allen and Pickering, 2002), convective available potential energy (Choi et al., 2005), or  
80 convectively induced updraft velocity (Allen et al., 2000; Allen and Pickering, 2002). More  
81 recently, Finney et al. (2014, 2016) adopted a lightning parameterization using upward cloud ice  
82 flux at 440hPa (based upon definitions of deep convective clouds in the International Satellite  
83 Cloud Climatology Project (Rossow et al., 1996)) and implemented it in the United Kingdom  
84 Chemistry and Aerosol model (UKCA). With the availability of lightning flash data from the



85 National Lightning Detection Network (NLDN) (Orville et al., 2002), recent LNO<sub>x</sub>  
86 parameterization schemes started to include the observed lightning flash information to constrain  
87 LNO<sub>x</sub> in regional Chemical Transport Models (CTMs) (Allen et al., 2012). In Kang et al. (2019),  
88 we described the existing LNO<sub>x</sub> parameterization scheme that is based on the monthly NLDN  
89 (mNLDN) lightning flash data, and an updated scheme using hourly NLDN (hNLDN) lightning  
90 flash data in the CMAQ lightning module. In addition, we also developed a scheme based on  
91 linear and log-linear regression parameters using multiyear NLDN observed lightning flashes  
92 and model predicted convective precipitation rate (pNLDN). The preliminary assessment of  
93 these schemes based on total column LNO<sub>x</sub> suggests that all the schemes provide reasonable  
94 LNO<sub>x</sub> estimates in time and space, but during summer months, the mNLDN scheme tends to  
95 produce the most and the pNLDN scheme the least LNO<sub>x</sub>.

96 The first study on the impact of LNO<sub>x</sub> on surface air quality using CMAQ was conducted  
97 by Allen et al. (2012) and followed by Wang et al. (2013) with different ways for parameterizing  
98 LNO<sub>x</sub> production and different model configurations. In this study, we present performance  
99 evaluations using each of the LNO<sub>x</sub> production schemes (mNLDN, hNLDN, pNLDN) described  
100 by Kang et al. (2019) to provide estimates of LNO<sub>x</sub> in CMAQ. In addition to examination of  
101 differences in air quality estimates between these schemes, we compare the model predictions to  
102 base model estimates without LNO<sub>x</sub> and evaluate the estimates from all of the simulations  
103 against surface and airborne observations.

104 Section 2 describes the model configuration, simulation scenarios, analysis methodology,  
105 and observational data. Section 3 presents the analysis results and Section 4 presents the  
106 conclusions.

107

## 108 **2. Methodology**

### 109 **2.1 The CMAQ model and simulation configurations**

110 The three LNO<sub>x</sub> production schemes described in Kang et al (2019) were incorporated  
111 into CMAQ v5.2 (Appel et al. 2017; doi:10.5281/zenodo.1167892). The chemical mechanism  
112 used was CB6 (Yarwood et al., 2010) and the aerosol module was AERO6 (Nolte et al., 2015).



113 The meteorological inputs were provided by the Weather Research and Forecasting (WRF)  
114 model version 3.8 and the model-ready meteorological input files were created using version 4.2  
115 of the meteorology–chemistry interface processor (MCIP; Otte and Pleim, 2010).

116 The modeling domain covers the entire contiguous United States (CONUS) and  
117 surrounding portions of northern Mexico and southern Canada, as well as the eastern Pacific and  
118 western Atlantic oceans. The model domain consists of 299 north–south grid cells by 459 east–  
119 west grid cells utilizing 12 km x 12 km horizontal grid spacing, 35 vertical layers with varying  
120 thickness extending from the surface to 50 hPa and an approximately 10m midpoint for the  
121 lowest (surface) model layer. The simulation time period covers the months from April to  
122 September 2011 with a 10-day spin-up period in March.

123 Emission input data were based on the 2011 National Emissions Inventory  
124 (<https://www.epa.gov/air-emissions-inventories>). The raw emission files were processed using  
125 version 3.6.5 of the Sparse Matrix Operator Kernel Emissions (SMOKE;  
126 <https://www.cmascenter.org/smoke/>) processor to create gridded speciated hourly model-ready  
127 input emission fields for input to CMAQ. Electric generating unit (EGU) emissions were  
128 obtained using data from EGUs equipped with a continuous emission monitoring system  
129 (CEMS). Plume rise for point and fire sources were calculated in-line for all simulations (Foley  
130 et al., 2010). Biogenic emissions were generated in-line in CMAQ using BEIS versions 3.61  
131 (Bash et al., 2016). All the simulations employed the bidirectional (bi-di) ammonia flux option  
132 for estimating the air–surface exchange of ammonia.

133 There are four CMAQ simulation scenarios for this study: 1) simulation without LNO<sub>x</sub>  
134 (Base), 2) simulation with LNO<sub>x</sub> generated by the scheme based on monthly information from  
135 the NLDN (mNLDN), 3) simulation with LNO<sub>x</sub> generated by scheme based on hourly  
136 information from the NLDN (hNLDN), and 4) simulation with LNO<sub>x</sub> generated by the scheme  
137 parameterizing lightning emissions based on modeled convective activity (pNLDN) as described  
138 in detail in Kang et al. (2019). All other model inputs, parameters and settings were the same  
139 across the four simulations. The vertical distribution algorithm is the same for all the LNO<sub>x</sub>  
140 schemes as also described in Kang et al. (2019).

141

142

143



## 144        **2.2 Observations and analysis techniques**

145        To assess the impact of LNO<sub>x</sub> on ground-level air quality, output from the various CMAQ  
146 simulations were paired in space and time with observed data from the EPA's Air Quality  
147 System (AQS; <https://www.epa.gov/aqs>) for hourly O<sub>3</sub> and NO<sub>x</sub>. To evaluate the vertical  
148 distribution, measurements of trace species from the Deriving Information on Surface Conditions  
149 from Column and Vertically Resolved Observations Relevant to Air Quality (DISCOVER-AQ;  
150 <http://www.nasa.gov/missions/discover-aq>) campaign conducted in the Baltimore/Washington  
151 region (e.g., Crawford and Pickering, 2014; Anderson et al., 2014; Follette-Cook et al., 2015)  
152 were used. During this campaign, the NASA P-3B aircraft measured trace gases including O<sub>3</sub>,  
153 NO, and NO<sub>2</sub>. Vertical profiles were obtained over seven locations – Beltsville (Be), Padonia  
154 (Pa), Fairhill (Fa), Aldino (Al), Edgewood (Ed), Essex (Es), and Chesapeake Bay (Cb) from  
155 approximately 0.3 to 5 km above ground level during P-3B flights over 14 days in July 2011.  
156 During this same period, ozonesonde measurements were taken that extended from ground level  
157 through the entire model column at two locations (Beltsville, MD and Edgewood, MD shown in  
158 Figure 1). Inclusion of LNO<sub>x</sub> estimates in the CTM simulations also has an important impact on  
159 model estimated wet deposition of nitrate. Therefore, assessment was also performed using data  
160 from the National Atmospheric Deposition Program's National Trends Network (NADP/NTN,  
161 <http://ndp.slh.wisc.edu/ntn>).

162        Since lightning activity as well as LNO<sub>x</sub> exhibit distinct spatial variations (Kang and  
163 Pickering, 2018), analysis was conducted for the model domain over the contiguous United  
164 States, and then for each region as shown in Figure 1. Emphasis is placed on two regions,  
165 Southeast (SE) and Rocky Mountains (RM), where lightning activity is more prevalent and  
166 LNO<sub>x</sub> has the greatest impact on model predictions as shown in Results - increasing model bias  
167 in the SE and decreasing bias in the RM. The commonly used statistical metrics, Root Mean  
168 Square Error (RMSE), Normalized Mean Error (NME), Mean Bias (MB), Normalized Mean  
169 Bias (NMB), and Correlation Coefficient (R), in the model evaluation field as defined in Kang et  
170 al. (2005) and Eder et al. (2006) were calculated to assess the basic performance differences  
171 among all the model cases for their ground-level air quality predictions.

172

173



174

175 **3. Results**176 **3.1 Ground-level evaluation for O<sub>3</sub> and NO<sub>x</sub>**177 **3.1.1 Statistical performance metrics**

178 Tables 1 and 2 display the statistical model performance metrics for daily maximum 8-hr  
179 (DM8HR) O<sub>3</sub> and daily mean NO<sub>x</sub> mixing ratios over the domain and each analysis region for  
180 all four model cases in July 2011 (Base, mNLDN, hNLDN, and pNLDN). The best performance  
181 metrics among the model cases are highlighted in bold. As shown in Table 1, for DM8HR O<sub>3</sub>,  
182 the Base simulation has the lowest MB and NMB values over the Domain, while hNLDN  
183 produced the smallest RMSE and NME values. mNLDN generated the largest values for both  
184 error (RMSE and NME) and biases (MB and NMB), followed by pNLDN. More importantly, all  
185 model cases with LNO<sub>x</sub> exhibit slightly higher correlation coefficients than the Base simulation,  
186 suggesting the importance of including the contributions of this source for improving the spatial  
187 and temporal variability in model predictions. Additionally, the hNLDN simulation exhibited  
188 higher correlation and lower bias and error relative to the measurements indicating the value of  
189 higher temporal resolution lightning activity for representing the associated NO<sub>x</sub> emissions and  
190 their impacts on tropospheric chemistry.

191 Examining the regional results for DM8HR O<sub>3</sub> in Table 1, the statistical measures indicate  
192 that in the Northeast (NE), hNLDN outperformed all other model cases with the lowest errors  
193 and biases and highest correlation coefficient. In Southeast (SE), the Base performed better with  
194 the lowest errors and mean biases, but the correlation coefficient (R) value for hNLDN is slightly  
195 higher. Among all the LNO<sub>x</sub> cases, mNLDN produced the worst statistics in this region.  
196 Historically, CTMs tend to significantly overestimate surface O<sub>3</sub> in the Southeast US (Lin et al.,  
197 2008; Fiore et al., 2009; Brown-Steiner et al., 2015; Canty et al., 2015), and this is speculated to  
198 be driven in part by an overestimation of anthropogenic NO<sub>x</sub> emission estimates. Thus, even  
199 though lightning is known to impact ambient air quality, including this additional NO<sub>x</sub> source  
200 can worsen model performance in some locations and time periods due to other errors in the  
201 modeling system. As noted in Table 1, for SE, the MB values increased by about 1.6 ppb in  
202 mNLDN and less than 1 ppb in hNLDN and pNLDN. Nevertheless, the correlation coefficients  
203 for mNLDN and pNLDN are almost the same with the Base, and hNLDN was slightly higher



204 (0.77 compared to 0.76). These correlations indicate that even though additional NO<sub>x</sub> increases  
205 the mean bias, when it is added correctly in time and space, as with the case of hNLDN, the  
206 spatial and temporal correlation are improved. In Upper Midwest (UM), the lowest errors and  
207 biases among the model cases are associated with hNLDN, while the worst performance is with  
208 mNLDN. In the Lower Midwest (LM), hNLDN performed comparable with the Base, with  
209 hNLDN having the highest correlation and lowest mean errors, while the Base has the lowest  
210 mean biases. Rocky Mountain (RM) is the only region that shows an underestimation of  
211 DM8HR O<sub>3</sub>. In this region all the model cases with LNO<sub>x</sub> outperformed the Base case in all the  
212 metrics. Among the three model cases with LNO<sub>x</sub>, mNLDN produced the lowest MB and NMB  
213 values, while hNLDN had the lowest RMSE and NME, and the highest correlation. In the Pacific  
214 Coast (PC) region, lightning activity is generally very low compared to other regions (Kang and  
215 Pickering, 2018). All model cases with LNO<sub>x</sub> outperformed the Base case, especially hNLDN  
216 which had the lowest mean error and bias and highest correlation among all the cases.

217 Most of the NO<sub>x</sub> produced by lightning is distributed in the middle and upper troposphere  
218 with only a small portion being distributed close to the surface. As a result, the impact on  
219 ground-level NO<sub>x</sub> mixing ratios is small. Table 2 shows all the model cases produced similar  
220 statistics for the daily mean NO<sub>x</sub> mixing ratios at AQS sites across the domain and within all the  
221 subregions. Although the changes in model performance are small, the model cases with LNO<sub>x</sub>  
222 exhibit similar or slightly better performance than the Base case.

### 223 3.1.2 Time series

224 Figure 2 presents the timeseries of regional-mean observed and modeled DM8HR O<sub>3</sub> for  
225 the entire domain and the SE and RM regions during July 2011. Over the domain and in SE, all  
226 the model cases overestimate the mean DM8HR O<sub>3</sub> mixing ratios on all days with the Base being  
227 the closest to the observations. hNLDN is almost the same as the Base with slightly higher  
228 values on some days. Among all the cases, mNLDN produced the highest values on almost all  
229 days through the month, on the order of 1-2 ppb higher than the Base. In contrast, in the RM  
230 region, the Base significantly underestimates DM8HR O<sub>3</sub> mixing ratios on all the days during  
231 the month, while all model cases with LNO<sub>x</sub> improved model predictions relative to  
232 observations in the region. Among the three model cases with LNO<sub>x</sub>, mNLDN produced the  
233 lowest bias for all the days, closely followed by hNLDN.





234 Figure 3 displays the average daily mean NO<sub>x</sub> mixing ratios at AQS sites over the same  
235 regions as in Figure 2. On most of the days in July 2011, over the domain and in SE, the model  
236 cases overestimate NO<sub>x</sub> values, and on almost half of the days, the overestimation is significant  
237 (up to 100%). As noted in Table 2, on average, the overestimation is ~17% over the domain and  
238 ~43% in SE. However, in RM, the predicted NO<sub>x</sub> mixing ratios closely follow the daily  
239 observations and on average the modeled and observed magnitude is almost identical (~3%  
240 difference). All the model cases, with or without LNO<sub>x</sub>, produced almost the same mean NO<sub>x</sub>  
241 mixing ratios at the surface. However, the different cases produce different levels of LNO<sub>x</sub> in the  
242 middle and upper troposphere, resulting in differences in O<sub>3</sub> production and transport which  
243 impact ground-level O<sub>3</sub> levels. We further explore these features in Section 3.2 which presents  
244 evaluation of modeled vertical pollutant distributions.

### 245 3.1.3 Diurnal variations

246 Diurnal plots are used to further examine differences in model evaluation for O<sub>3</sub> and  
247 NO<sub>x</sub>. Figure 4 shows the mean diurnal profiles for hourly O<sub>3</sub> and NO<sub>x</sub> over the entire domain,  
248 SE, and RM. On a domain mean basis, all model cases overestimate O<sub>3</sub> during the daytime  
249 hours, while in the SE, the overestimation spans all the hours. In RM, the model cases  
250 significantly underestimate O<sub>3</sub> across all the hours except for a few early morning hours, when  
251 the model predicted values are very close to the observations. Among all the model cases, as  
252 expected, the most prominent differences occurred during the midday hours when the  
253 photochemistry is most active. However, the difference between hNLDN (and mNLDN) and the  
254 Base is also significant during the night in the RM region, even though the O<sub>3</sub> levels are low.  
255 This may be attributed to NO<sub>x</sub>-related nighttime chemistry in part caused by freshly released NO  
256 by cloud-to-ground lightning flashes. The diurnal variations of NO<sub>x</sub> are similar over the domain  
257 and in the regions for all model cases. Appel et al. (2017) reported a significant overestimation of  
258 NO<sub>x</sub> mixing ratios at AQS sites during nighttime hours and underestimation during daytime  
259 hours. The bias pattern is identical for all of the LNO<sub>x</sub> model cases evaluated here (Figure 4).

### 260 3.1.4 Spatial variations

261 Figure 5 shows the impact of the different LNO<sub>x</sub> schemes on model performance for  
262 DM8HR O<sub>3</sub> at AQS sites. The spatial maps show the difference in absolute MB between the



263 cases with lightning NO<sub>x</sub> emissions and the Base and is calculated as follows. First, the absolute  
264 MB was calculated at each site for each case, e.g.  $|MB_{[Base-Obs]}|$ , then the difference in absolute  
265 MB was calculated between model cases, e.g.  $|MB_{[hNLDN-Obs]}| - |MB_{[Base-Obs]}|$ . The histograms of  
266 the differences in absolute MB between model cases in Figure 5 are provided to show the  
267 distribution of the change in model performance across space, i.e. the frequency of an  
268 improvement in model performance versus a degradation in model performance between cases.  
269 As shown in Figure 5, the mNLDN shows increased model bias in the east US and along the  
270 California coast, but reduced model bias in the RM. At a majority of the AQS sites, it increases  
271 the model bias (only decreases at 26.8% (346) of the sites). The hNLDN also significantly  
272 reduces model bias in the RM with a moderate increase in the SE. Overall, in the hNLDN, the  
273 mean bias decreased at 61.2% (791) of AQS sites. Similar to mNLDN, increases in mean bias  
274 are noted at 29.3% (378) of the AQS sites in the pNLDN simulation. As noted in the histograms,  
275 the distribution of the model bias in the pNLDN is much narrower than both mNLDN and  
276 hNLDN, eliminating the large bias increases in mNLDN and the significant bias decreases in  
277 hNLDN.

## 278 **3.2 Vertical evaluation for O<sub>3</sub> and NO<sub>x</sub>**

### 279 **3.2.1 Ozone-sonde observations**

280 A large source of uncertainty in the specification of LNO<sub>x</sub> is its vertical allocation, which  
281 can impact the model's ability to accurately represent the variability in both chemistry and  
282 transport. To further assess the impact of the vertical LNO<sub>x</sub> specification on model results, we  
283 compared vertical profiles of simulated model O<sub>3</sub> with extensive ozonesonde measurements  
284 available during the study period. Figure 6 presents the vertical profiles for O<sub>3</sub> sonde  
285 measurements and paired model estimates of all model cases at Beltsville, MD and Edgewood,  
286 MD. At each location, observations from multiple days are available (one or two soundings per  
287 day) during the 2011 DISCOVER-AQ campaign in July 2011. The model evaluation was limited  
288 to days where the inclusion of LNO<sub>x</sub> has an obvious impact (the vertical profile lines can be  
289 separated) on the model estimates (July 21, 22, 28 and 29 at Beltsville, and July 21, 22, 28, 29,  
290 and 30 at Edgewood). We paired the observed data with model estimates in time and space and  
291 averaged the model and observed values at each model layer. Only data below 12 km altitude are  
292 plotted in Figure 6 to exclude possible influence of stratospheric air on O<sub>3</sub>. As can be seen in



293 Figure 6, at both locations the Base case underestimates O<sub>3</sub> mixing ratios from around 1 km  
294 upwards, but overestimates closer to the surface. When LNO<sub>x</sub> is included in the simulations, the  
295 predicted O<sub>3</sub> mixing ratios increase relative to the Base case starting around 2km, with greater  
296 divergence from the Base case at higher altitudes. The two model cases, hNLDN and mNLDN,  
297 produced similar O<sub>3</sub> levels until about 6 km, but above that altitude the mNLDN ozone mixing  
298 ratios were higher. All the model cases with LNO<sub>x</sub> performed much better aloft than the Base  
299 case. Near the surface, all the model cases overestimated O<sub>3</sub>, however hNLDN had smaller bias  
300 than the other simulations. This may be attributed to the fact that only hNLDN used the observed  
301 lightning flash data directly, and as a result, LNO<sub>x</sub> was estimated more accurately in time and  
302 space. This improvement in model bias at the surface is further investigated in the next section  
303 using evaluation against P-3B measurements.

### 304 3.2.2 P-3B measurement

305 Extensive measurements of lower tropospheric chemical composition distributions over  
306 the Northeastern U.S. are available from instruments onboard the P-3B aircraft on 14 days of the  
307 DISCOVER-AQ campaign. We utilize measurements from one of the days (28 July 2011) with  
308 noticeable (the mean vertical profiles of LNO<sub>x</sub> cases are separable from that of the base case)  
309 lightning impacts, to evaluate the model simulations. Figure 7 shows measured O<sub>3</sub> mixing ratios  
310 overlaid on the modeled vertical time-section for 1030 – 1730 UTC. The color-filled circles  
311 represent measured O<sub>3</sub> mixing ratios averaged over 60 seconds and the background is the model  
312 estimated vertical profiles from the grid cells containing the P-3B flight path for that hour and  
313 location. As indicated in the Base case (Figure 7a), the model tends to overestimate O<sub>3</sub> mixing  
314 ratios from the surface to about 2 km, but underestimate at altitudes above 2 km. The hNLDN  
315 reduced the overestimation below 2km, e.g. fewer grid cells with mixing ratios above 90ppb  
316 (shown in red). The other two cases (mNLDN, pNLDN) did not produce the same improvement  
317 near the surface. The hNLDN also decreases the underestimation aloft compared to the Base case  
318 with O<sub>3</sub> mixing ratios in the 55-65 ppb range (light blue colors), better matching the measured  
319 values. This decrease in underestimation aloft is also seen in the mNLDN case, but to a lesser  
320 degree while the pNLDN case shows only slight improvement aloft over the Base simulation.

321 To further differentiate the three LNO<sub>x</sub> model cases, Figures 8-10 show the difference in  
322 the time-sections between each of the model cases with LNO<sub>x</sub> and the Base for NO, NO<sub>x</sub>, and



323 O<sub>3</sub> from all the model layers along the P-3B flight path on July 28. As seen in Figure 8, the  
324 hNLDN scheme injected most NO above 5 km and small amount near the surface, with the  
325 maximum amount injected between 13-14 km. After release into the atmosphere, NO is quickly  
326 converted into NO<sub>2</sub> in the presence of O<sub>3</sub>, and these collectively result in the NO<sub>x</sub> (NO+NO<sub>2</sub>)  
327 vertical time-section (local production plus transport) shown in the middle panel of Figure 8.  
328 NO<sub>x</sub> is further mixed down through the time-section and more persistent along the flight path  
329 near the surface than is NO. As a result, significant O<sub>3</sub> is produced above 3 km and the maximum  
330 O<sub>3</sub> difference appears between 9 and 14 km during the early afternoon hours (from 13:30 to  
331 17:30). However, from surface to about 2 km, O<sub>3</sub> is reduced consistently across the entire period,  
332 and this is the result of O<sub>3</sub> titration by NO from cloud-to-ground lightning flashes that must have  
333 been transported to this layer by storm downdrafts. Since O<sub>3</sub> is significantly underestimated  
334 above 3 km and overestimated near the surface by the Base model, the inclusion of LNO<sub>x</sub>  
335 greatly improved the model's performance under both conditions.

336 Comparison of Figure 9 (mNLDN) with Figure 8 (hNLDN) reveals that the time-sections  
337 of NO and NO<sub>x</sub> above 5 km are similar for these two cases, but they are dramatically different  
338 near the surface. The near-surface increase in ambient NO noted in the hNLDN is absent in  
339 mNLDN, and in fact there are some small decreases in NO, although the reason for this is  
340 unclear. The increase in O<sub>3</sub> aloft in the mNLDN case is similar to that seen in the hNLDN case.  
341 However, the near-surface reduction in O<sub>3</sub> is almost absent. In the pNLDN case (Figure 10), NO  
342 mixing ratios are much less than those in hNLDN and mNLDN in the upper layers as a result of  
343 less column NO being generated by the linear parameterization. The resulting NO<sub>x</sub> time-section  
344 is also smoothed. The pNLDN time-sections for NO, NO<sub>x</sub> and O<sub>3</sub> near the surface are similar to  
345 the mNLDN case with no change or small decreases compared to the Base case. O<sub>3</sub> mixing ratios  
346 increase by more than 30 ppb during the afternoon hours between 10 – 13 km in the pNLDN  
347 case, however the increase is not as intense and widespread as the other cases. In summary, the  
348 hNLDN scheme produces estimates that are more consistent with measurements at the surface  
349 and aloft, compared to the other simulations, reflecting the advantage of using the spatially and  
350 temporally-resolved observed lightning flash data. The model performance improvement for  
351 simulated O<sub>3</sub> distributions also suggests robustness in the vertical distribution scheme when  
352 LNO<sub>x</sub> is generated at the right time and location.



353 To corroborate the above time-section distributions of NO, NO<sub>x</sub>, and O<sub>3</sub> in the lightning  
354 cases, the lightning NO emissions are traced back on July 28 for each case. It is found that in all  
355 cases, the lightning NO was injected about 200 km upwind (north-west) of the flight path. The  
356 hNLDN case captured two injections: one occurred during the morning hours (5:00 to 7:00 am)  
357 and the other happened during the afternoon hours (after 2:30 pm). Both mNLDN and pNLDN  
358 captured the afternoon lightning event at the later time (after 3:30 pm for mNLDN and after 4:30  
359 pm for pNLDN) with varying intensity, but neither captured the morning lightning event, which  
360 explains why the increase of NO and NO<sub>x</sub> in the hNLDN case (Figure 8) did not occur in the  
361 mNLDN and pNLDN cases (Figures 9 and 10). Also note that the significant increase of NO  
362 during the time period from 11:00 to 13:00 occurred about 5 hours after the lightning NO was  
363 injected at about 200 km upwind in the hNLDN case.

364 To expand on the evaluation in Figures 7-10 which focused on measurements from July  
365 28, 2011, we retrieved all the P-3B measurements on days with noticeable lightning impact (July  
366 21, 22, 28, and 29). The 3-D paired observation-model data were grouped together by spiral site  
367 and the mean biases (model – observation) were plotted in Figure 11 (a and b) for O<sub>3</sub> and NO,  
368 respectively. The boxplots for O<sub>3</sub> in Figure 11a suggests that the Base exhibited larger bias with  
369 greater spread (i.e. larger interquartile range) than other model cases incorporating LNO<sub>x</sub> at most  
370 of the locations where aircraft spirals were conducted. At all locations except Aldino, the lowest  
371 mean biases in simulated NO and O<sub>3</sub> are noted in the hNLDN simulation.

372

### 373 **3.3 Deposition evaluation for nitrate**

374 In addition to contributing to tropospheric O<sub>3</sub> formation, NO<sub>x</sub> oxidation also leads to gaseous  
375 nitric acid and particulate-nitrate which are eventually removed from the atmosphere by dry and  
376 wet deposition of nitrate (NO<sub>3</sub><sup>-</sup>). As a result, inclusion of NO<sub>x</sub> from lightning also plays an  
377 important role in nitrogen deposition modeling. To assess the impacts of incorporating LNO<sub>x</sub>  
378 emissions on simulated oxidized nitrogen deposition, we compared model estimated amounts of  
379 precipitation from NTN network (<http://nadp.slh.wisc.edu/ntn/>) and wet deposition of NO<sub>3</sub><sup>-</sup> with  
380 measurements from the NADP network (<http://nadp.slh.wisc.edu/>). During summer months in  
381 2011 (June -August) the WRF model generally reproduces the observed precipitation with a  
382 slight underestimate in the east, but the Base model simulation tends to underestimate wet



383 deposition of  $\text{NO}_3^-$  across the domain, with the greatest underestimation in the SE and UM (See  
384 Table 3 and Figure 12). All three LNO<sub>x</sub> simulations increase wet deposition amounts of  $\text{NO}_3^-$   
385 and decrease model bias in all regions. The bottom panel of Figure 12 shows that the mNLDN  
386 simulation resulted in the largest increase over the base model estimates. The NMB is reduced  
387 from -35% in the Base to -15% in mNLDN across the domain and from -32% to -2% in the SE.  
388 The hNLDN shows very similar model performance to the mNLDN case. In contrast, the wet  
389 deposition  $\text{NO}_3^-$  estimates from the pNLDN case are only slightly higher than the Base case, and  
390 as a result the evaluation statistics for pNLND are very similar to the Base statistics. As  
391 discussed earlier, the mNLDN tends to produce the most LNO<sub>x</sub> among the three LNO<sub>x</sub> schemes,  
392 thus it results in the smallest errors in terms of wet deposition of  $\text{NO}_3^-$  when compared to the  
393 Base simulation that significantly underestimated  $\text{NO}_3^-$  wet deposition. It should be noted that in  
394 addition to the LNO<sub>x</sub> contributions, errors in modeled precipitation amounts and patterns also  
395 likely influence the underestimation of  $\text{NO}_3^-$  wet deposition.

396

#### 397 **4. Conclusions**

398 A detailed evaluation of lightning NO<sub>x</sub> emission estimation parameterizations available  
399 in the CMAQ modeling system was performed through comparisons of model simulation  
400 results with surface and aloft air quality measurements.

401 Our analysis indicates that incorporation of LNO<sub>x</sub> emissions enhanced O<sub>3</sub> production in  
402 the middle and upper troposphere, where O<sub>3</sub> mixing ratios were often significantly  
403 underestimated without the representation of LNO<sub>x</sub>. Though the impact on surface O<sub>3</sub> varies  
404 from region to region and is also dependent on the accuracy of the NO<sub>x</sub> emissions from other  
405 sources, the inclusion of LNO<sub>x</sub>, when it is injected at the appropriate time and location, can  
406 improve the model estimates. In regions where the base model estimates of O<sub>3</sub> were biased  
407 high, the inclusion of LNO<sub>x</sub> further increased the model bias; and a systematic increase is  
408 noted in the correlation with measurements, suggesting that emissions from other sources  
409 likely drive the overestimation. Identifying how errors in emissions inputs from different  
410 sources interact with errors in meteorological modeling of mixing and transport, remains a  
411 challenging but critical task. Likewise, all the LNO<sub>x</sub> schemes also enhanced the accumulated



412 wet deposition of  $\text{NO}_3^-$ , that was significantly underestimated by the base model without  
413 LNO<sub>x</sub> throughout the modeling domain except the Pacific Coast.

414 Uncertainty remains in modeling the magnitude and spatial, temporal and vertical  
415 distribution of lightning produced NO<sub>x</sub>. LNO<sub>x</sub> schemes are built on numerous assumptions  
416 and all current schemes also depend on the skill of the upstream meteorological models in  
417 describing convective activity. Nevertheless, these schemes reflect our best understanding  
418 and knowledge at the time when the schemes were implemented. The use of hourly  
419 information on lightning activity yielded LNO<sub>x</sub> emissions that generally improved model  
420 performance for ambient O<sub>3</sub> and NO<sub>x</sub> as well as oxidized nitrogen wet deposition amounts.  
421 As more high-quality data from both ground and satellite measurements become available,  
422 the performance of the LNO<sub>x</sub> schemes will continue to improve.

423

#### 424 **Code and data availability**

425 CMAQ model documentation and released versions of the source code, including all model  
426 code used in his study, are available at <https://www.epa.gov/cmaq>. The data processing and  
427 analysis scripts are available upon request. The WRF model is available for download through  
428 the WRF website (<http://www.wrf-model.org/index.php>).  
429 The raw lightning flash observation data used are not available to the public but can be  
430 purchased through Vaisala Inc. ([https://www.vaisala.com/en/products/systems/lightning-](https://www.vaisala.com/en/products/systems/lightning-detection)  
431 [detection](https://www.vaisala.com/en/products/systems/lightning-detection)). The immediate data behind the tables and figures are available from  
432 <https://zenodo.org/record/2621096> (Kang and Foley, 2019). Additional input/output data for  
433 CMAQ model utilized for this analysis are available upon request as well.

434

435

436 **Disclaimer:** The views expressed in this paper are those of the authors and do not necessarily  
437 represent the views or policies of the U.S. EPA.

438

#### 439 **Author Contribution**

440 **Daiwen Kang:** data collection, algorithm design, model simulation, analysis, and manuscript  
441 writing.

442 **Kristen Foley:** data analysis and manuscript writing.

443 **Rohit Mathur:** manuscript editing.

444 **Shawn Roselle:** manuscript editing.



445 **Kenneth Pickering:** manuscript editing.

446 **Dale Allen:** manuscript editing.

447

#### 448 **Acknowledgement:**

449 The authors thank Brian Eder, Golam Sarwar, and Janet Burke (U.S. /EPA) for their  
450 constructive comments and suggestions during the internal review process.

451

#### 452 **References**

- 453 Allen, D., Pickering, K., Stenchikov, G., Thompson, A., and Kondo, Y.: A three-dimensional  
454 total odd nitrogen (NO<sub>y</sub>) simulation during SONEX using a stretched-grid chemical  
455 transport model, *J. Geophys. Res.*, 105, 3851–3876, doi:10.1029/1999JD901029, 2000.
- 456 Allen, D. J. and Pickering, K. E.: Evaluation of lightning flash rate parameterizations for use in a  
457 global chemical transport model, *J. Geophys. Res.*, 107, 4711,  
458 doi:10.1029/2002JD002066, 2002.
- 459 Allen, D. J., Pickering, K. E., Pinder, R. W., Henderson, B. H., Appel, K. W., and Prados, A.:  
460 Impact of lightning-NO on eastern United States photochemistry during the summer of  
461 2006 as determined using the CMAQ model, *Atmos. Chem. Phys.*, 12, 1737–1758,  
462 doi:10.5194/acp-12-1737-2012, 2012.
- 463 Anderson, D. C., Loughner, C. P., Diskin, G., Weinheimer, A., Canty, T. P., Salawitch, R. J.,  
464 Worden, H. M., Fried, A., Mikoviny, T., Wisthaler, A., and Dickerson, R. R.: Measured  
465 and modeled CO and NO<sub>y</sub> in DISCOVER-AQ: An evaluation of emissions and  
466 chemistry over the eastern US, *Atmos. Environ.*, 96, 78-87,  
467 doi:10.1016/j.atmosenv.2014.07.004, 2014.
- 468 Appel, K. W., Napelenok, S. L., Foley, K. M., Pye, H. O., Hogrefe, C., Luecken, D. J., Bash, J.  
469 O., Roselle, S. J., Pleim, J. E., Foroutan, H., Hutzell, W. D., Pouliot, G. O., Sarwar, G.,  
470 Fahey, K. M., Gantt, G., Gilliam, R. C., Heath, N. K., Kang, D., Mathur, R., Schwede, D.  
471 B., Spero, T. L., Wong, D. C., and Young, J. O.: Description and evaluation of the  
472 Community Multiscale Air Quality (CMAQ) modeling system version 5.1, *Geosci.*  
473 *Model Dev.*, 10, 1703–1732, doi:10.5194/gmd-10-1703-2017, 2017.
- 474 Appel, K. W., Foley, K. M., Bash, J. O., Pinder, R. W., Dennis, R. L., Allen, D. J., and  
475 Pickering, K.: A multi-resolution assessment of the Community Multiscale Air Quality  
476 (CMAQ) model v4.7 wet deposition estimates for 2002–2006, *Geosci. Model Dev.*, 4,  
477 357–371, doi:10.5194/gmd-4-357-2011, 2011.





- 478 Bash, J. O., Baker, K. R., and Beaver, M. R.: Evaluation of improved land use and canopy  
479 representation in BEIS v3.61 with biogenic VOC measurements in California, *Geosci.*  
480 *Model Dev.*, 9, 2191–2207, doi:10.5194/gmd-9-2191-2016, 2016.
- 481 Bovensmann, H., Burrows, J. P., Buchwitz, M., Frerick, J., No`el, S., Rozanov, V. V., Chance,  
482 K. V., and Goede, A. P. H.: SCIAMACHY: Mission Objectives and Measurement  
483 Modes, *J. Atmos. Sci.*, 56, 127–150, 1999.c
- 484 Brown-Steiner, B., Hess, P. G., and Lin, M. Y.: On the capabilities and limitations of GCCM  
485 simulations of summertime regional air quality: A diagnostic analysis of ozone and  
486 temperature simulations in the US using CESM CAM-Chem, *Atmos. Environ.*, 101, 134–  
487 148, doi:10.1016/j.atmosenv.2014.11.001, 2015
- 488 Byun, D. W. and Schere, K. L.: Review of the governing equations, computational algorithms,  
489 and other components of the Models-3 Community Multiscale Air Quality (CMAQ)  
490 modeling system, *Appl. Mech. Rev.*, 59, 51-77, 2006.
- 491 Canty, T. P., Hemberck, L., Vinciguerra, T. P., Anderson, D. C., Goldberg, D. L., Carpenter, S.  
492 F., Allen, D. J., Loughner, C. P., Salawitch, R. J., and Dickerson, R. R.: Ozone and NOx  
493 chemistry in the eastern US: evaluation of CMAQ/CB05 with satellite (OMI) data,  
494 *Atmos. Chem. Phys.*, 15, 10965–10982, doi:10.5194/acp-15-10965-2015, 2015.
- 495 Choi, Y., Wang, Y., Zeng, T., Martin, R. V., Kurosu, T. P., and Chance, K.: Evidence of  
496 lightning NOx and convective transport of pollutants in satellite observations over North  
497 America, *Geophys. Res. Lett.*, 32, L02805, doi:10.1029/2004GL021436, 2005.
- 498 Crawford, J. H. and Pickering, K. E.: DISCOVER-AQ: Advancing strategies for air quality  
499 observations for the next decade, EM, A&WMA, September, 2014.
- 500 Eder, B. K., Kang, D., Mathur, R., Yu, S., and Schere, K.: An operational evaluation of the Eta-  
501 CMAQ air quality forecast model, *Atmos. Environ.*, 40, 4894-4905, 2006.
- 502 Finney, D. L., Doherty, R. M., Wild, O., Huntrieser, H., Pumphrey, H. C., and Blyth, A. M.:  
503 Using cloud ice flux to parametrize large-scale lightning, *Atmos. Chem. Phys.*, 14,  
504 12665–12682, doi:10.5194/acp-14-12665-2014, 2014.
- 505 Finney, D. L., Doherty, R. M., Wild, O., and Abraham, N. L.: The impact of lightning on  
506 tropospheric ozone chemistry using a new global lightning parameterization, *Atmos.*  
507 *Chem. Phys.*, 16, 7507–7522, doi:10.5194/acp-16-7507-2016, 2016.
- 508 Flatøy, F. and Hov, O.: NOx from lightning and the calculated chemical composition of the free  
509 troposphere, *J. Geophys. Res.*, 102, 21 373–21 381, 1997.
- 510 Fiore, A. M., Dentener, F. J., Wild, O., Cuvelier, C., Schultz, M. G., Hess, P., Textor, C., Schulz,  
511 M., Doherty, R. M., Horowitz, L. W., MacKenzie, I. A., Sanderson, M. G., Shindell, D.  
512 T., Stevenson, D. S., Szopa, S., Van Dingenen, R., Zeng, G., Atherton, C., Bergmann, D.,  
513 Bey, I., Carmichael, G., Collins, W. J., Duncan, B. N., Faluvegi, G., Folberth, G., Gauss,  
514 M., Gong, S., Hauglustaine, D., Holloway, T., Isaksen, I. S. A., Jacob, D. J., Jonson, J. E.,



- 515 Kaminski, J. W., Keating, T. J., Lupu, A., Marmer, E., Montanaro, V., Park, R. J., Pitari,  
516 G., Pringle, K. J., Pyle, J. A., Schroeder, S., Vivanco, M. G., Wind, P., Wojcik, G., Wu,  
517 S., and Zuber, A.: Multimodel estimates of intercontinental source-receptor relationships  
518 for ozone pollution, *J. Geophys. Res.*, 114, D04301, doi:10.1029/2008jd010816, 2009.
- 519 Foley, K. M., Roselle, S. J., Appel, K. W., Bhave, P. V., Pleim, J. E., Otte, T. L., Mathur, R.,  
520 Sarwar, G., Young, J. O., Gilliam, R. C., Nolte, C. G., Kelly, J. T., Gilliland, A. B., and  
521 Bash, J. O.: Incremental testing of the Community Multiscale Air Quality (CMAQ)  
522 modeling system version 4.7, *Geosci. Model Dev.*, 3, 205–226, doi:10.5194/gmd-3-205-  
523 2010, 2010.
- 524 Follette-Cook, M. B., Pickering, K. E., Crawford, J. H., Duncan, B. N., Loughner, C. P., Diskin,  
525 G. S., Fried, A., and Weinheimer, A. J.: Spatial and temporal variability of trace gas  
526 columns derived from WRF/Chem regional model output: Planning for geostationary  
527 observations of atmospheric composition, *Atmos. Environ.*, 118, 28–44,  
528 doi:10.1016/j.atmosenv.2015.07.024, 2015.
- 529 Huntrieser, H., Schlager, H., Lichtenstern, M., Stock, P., Hamburger, T., Holler, H., Schmidt, K.,  
530 Betz, H. D., Ulanovsky, A., and Ravegnani, F.: Mesoscale convective systems observed  
531 during AMMA and their impact on the NO<sub>x</sub> and O<sub>3</sub> budget over West Africa. *Atmos*  
532 *Chem Phys.*, 11(6):2503–2536. doi:10.5194/acp-11-2503-2011, 2011.
- 533 Kang, D., Eder, B. K., Stein, A. F., Grell, G. A., Peckham, S. E., and Mcherry, J.: The New  
534 England air quality forecasting pilot program: development of an evaluation protocol and  
535 performance benchmark, *J. Air & Waste Manage. Assoc.*, 55, 1782–1796, 2005.
- 536 Kang, D., and Foley, K.: Simulating Lightning NO<sub>x</sub> Production in CMAQv5.2: Performance  
537 Evaluations, data set, <https://doi.org/10.5281/zenodo.2621096>, 2019.
- 538 Kang, D., Heath, N., Foley, K., Bash, J., Roselle, S., and Mathur, R.: On the relationship  
539 between observed NLDN lightning strikes and modeled convective precipitation rates:  
540 parameterization of lightning NO<sub>x</sub> production in CMAQ, *Air Pollution Modeling and its*  
541 *Application XXV*, Chapter 65, ISBN 978-3-319-57644-2, doi: 10.1007/978-3-319-  
542 57645-9, 2018.
- 543 Kang, D., Heath, N., Wong, D., Pleim, J., Roselle, S. J., Foley, K. M., and Mathur, R.: Lightning  
544 NO<sub>x</sub> Production in CMAQ: Part I – Using hourly NLDN Lightning Strike Data,  
545 Presented at 15th Annual CMAS Models-3 Users' Conference, 24–26 October 2016,  
546 UNC-Chapel Hill, available at:  
547 [https://www.cmascenter.org/conference/2016/slides/kang\\_lightning\\_nox\\_2016.pptx](https://www.cmascenter.org/conference/2016/slides/kang_lightning_nox_2016.pptx),  
548 2016.
- 549 Kang, D., Pickering, K. E., Allen, D. J., Foley, K. M., Wong, D., Mathur, R., and Roselle, S. J.:  
550 Simulating Lightning NO<sub>x</sub> Production in CMAQ: Evolution of Scientific Updates,  
551 *Geosci. Model Dev. Disc.*, doi:10.5194/gmd-2019-33, 2019.



- 552 Kang, D. and Pickering, K. E.: Lightning NO<sub>x</sub> emissions and the Implications for Surface Air  
553 Quality over the Contiguous United States, EM, A&WMA, November, 2018.
- 554 Kaynak, B., Hu, Y., Martin, R. V., Russell, A. G., Choi, Y., and Wang, Y.: The effect of  
555 lightning NO<sub>x</sub> production on surface ozone in the continental United States. *Atmos Chem*  
556 *Phys.* 8(17):5151–5159. doi:[10.5194/acp-8-5151-2008](https://doi.org/10.5194/acp-8-5151-2008), 2008.
- 557 Koo, B., Chien, C. J., Tonnesen, G., Morris, R., Johnson, J., Sakulyanontvittaya T.,  
558 Piyachaturawat, P., and Yarwood, G.: Natural emissions for regional modeling of  
559 background ozone and particulate matter and impacts on emissions control strategies.  
560 *Atmos Environ.*,44(19):2372–2382. doi:[10.1016/j.atmosenv.2010.02.041](https://doi.org/10.1016/j.atmosenv.2010.02.041), 2010.
- 561 Koshak, W., Peterson, H., Biazar, A., Khan, M., and Wang, L.: The NASA Lightning Nitrogen  
562 Oxides Model (LNOM): Application to air quality modeling, *Atmos. Res.*,  
563 doi:[10.1016/j.atmosres.2012.12.015](https://doi.org/10.1016/j.atmosres.2012.12.015), 2014.
- 564 Labrador, L. J., von Kuhlmann, R., and Lawrence, M. G.: The effects of lightning-produced NO<sub>x</sub>  
565 and its vertical distribution on atmospheric chemistry: sensitivity simulations with  
566 MATCHMPIC, *Atmos. Chem. Phys.*, 5, 1815–1834, 2005,
- 567 Lin, J., Youn, D., Liang, X., and Wuebbles, D.: Global model simulation of summertime U.S.  
568 ozone diurnal cycle and its sensitivity to PBL mixing, spatial resolution, and emissions,  
569 *Atmos. Environ.*, 42, 8470–8483, doi:[10.1016/j.atmosenv.2008.08.012](https://doi.org/10.1016/j.atmosenv.2008.08.012), 2008.
- 570 Murray, L. T.: Lightning NO<sub>x</sub> and Impacts on Air Quality, *Curr Pollution Rep.*, doi:  
571 [10.1007/s40726-016-0031-7](https://doi.org/10.1007/s40726-016-0031-7), 2016.
- 572 Nolte, C. G., Appel, K. W., Kelly, J. T., Bhave, P. V., Fahey, K. M., Collett Jr., J. L., Zhang, L.,  
573 and Young, J. O.: Evaluation of the Community Multiscale Air Quality (CMAQ) model  
574 v5.0 against size-resolved measurements of inorganic particle composition across sites in  
575 North America, *Geosci. Model Dev.*, 8, 2877–2892, doi:[10.5194/gmd-8-2877-2015](https://doi.org/10.5194/gmd-8-2877-2015),  
576 2015.
- 577 Napelenok, S. L., Pinder, R. W., Gilliland, A. B., and Martin, R. V.: A method for evaluating  
578 spatially-resolved NO<sub>x</sub> emissions using Kalman filter inversion, direct sensitivities, and  
579 spacebased NO<sub>2</sub> observations, *Atmos. Chem. Phys.*, 8, 5603–5614, doi:[10.5194/acp-8-5603-2008](https://doi.org/10.5194/acp-8-5603-2008), 2008.
- 581 Novak, J. H. and Pierce, T. E.: Natural emissions of oxidant precursors, *Water Air Soil Poll.*, 67,  
582 57-77, 1993.
- 583 Orville, R. E., Huffines, G. R., Burrows, W. R., Holle, R. L., and Cummins, K. L.: The North  
584 American Lightning Detection Network (NALDN) – first results: 1998-2000, *Mon. Wea.*  
585 *Rev.*, 130, 2098–2109, 2002.
- 586 Otte, T. L. and Pleim, J. E.: The Meteorology-Chemistry Interface Processor (MCIP) for the  
587 CMAQ modeling system: updates through MCIPv3.4.1, *Geosci. Model Dev.*, 3, 243–256,  
588 doi:[10.5194/gmd-3-243-2010](https://doi.org/10.5194/gmd-3-243-2010), 2010.



- 589 Pickering, K. E., Bučsela, E., Allen, D., Ring, A., Holzworth, R., and Krotkov, N.: Estimates of  
590 lightning NO<sub>x</sub> production based on OMI NO<sub>2</sub> observations over the Gulf of Mexico, J.  
591 Geophys. Res. Atmos., 121, 8668–8691, doi:10.1002/2015JD024179, 2016.
- 592 Price, C., Penner, J., and Prather, M.: NO<sub>x</sub> from lightning. 2. Constraints from the global  
593 atmospheric electric circuit, J. Geophys. Res., 102, 5943–5951, doi:10.1029/96JD02551, 1997.
- 594 Price, C. and Rind, D.: A simple lightning parameterization for calculating global lightning  
595 distributions, J. Geophys. Res., 97, 9919–9933, doi:10.1029/92JD00719, 1992.
- 596 Richter, A., Burrows, J. P., N<sup>o</sup>uß, H., Granier, C., and Niemeier, U.: Increase in tropospheric  
597 nitrogen dioxide over China observed from space, Nature, 437, 129–132,  
598 doi:10.1038/nature04092, 2005.
- 599 Rossow, W. B., Walker, A. W., Beuschel, D. E., and Roiter, M. D.: International Satellite Cloud  
600 Climatology Project (ISCCP) documentation of new cloud data sets, Tech. Rep. January,  
601 World Meteorological Organisation, WMO/TD 737, Geneva, 1996.
- 602 Schumann, U. and Huntrieser, H.: The global lightning-induced nitrogen oxides source, Atmos.  
603 Chem. Phys., 7, 3823–3907, doi:10.5194/acp-7-3823-2007, 2007.
- 604 Sioris, C. E., Kurosu, T. P., Martin, R. V., and Chance, K.: Stratospheric and tropospheric NO<sub>2</sub>  
605 observed by SCIAMACHY: first results, Adv. Space Res., 34, 780–785, 2004.
- 606 Stockwell, D. Z., Giannakopoulos, C., Plantevin, P. H., Carver, G. D., Chipperfield, M. P., Law,  
607 K. S., Pyle, J. A., Shallcross, D. E., and Wang, K. Y.: Modelling NO<sub>x</sub> from lightning and  
608 its impact on global chemical fields, Atmos. Environ., 33, 4477–4493, 1999.
- 609 Smith, S. N., and Mueller, S. F.: Modeling natural emissions in the Community Multiscale Air  
610 Quality (CMAQ) Model-I: building an emissions data base. Atmos Chem Phys.,  
611 10(10):4931–4952. doi:10.5194/acp-10-4931-2010, 2010.
- 612 Simon, H., Reff, A., Wells, B., Xing, J., and Frank, N.: Ozone trends across the United States  
613 over a period of decreasing NO<sub>x</sub> and VOC emissions. Environ. Sci. Technol., 49, 186-  
614 195, 2015.
- 658 Wang, L., Newchurch, M. J., Pour-Biazar, A., Kuang, S., Khan, M., Liu, X., Koshak, W., and  
659 Chance, K.: Estimating the influence of lightning on upper tropospheric ozone using  
660 NLDN lightning data and CMAQ model, Atmos. Environ., 67, 219–228, 2013.
- 661 Yarwood, G., Whitten, G. Z., Jung, J., Heo, G., and Allen, D. T.: Final Report: Development,  
662 Evaluation and Testing of Version 6 of the Carbon Bond Chemical Mechanism (CB6),  
663 available at:  
664 [https://www.tceq.texas.gov/assets/public/implementation/air/am/contracts/reports/pm/582](https://www.tceq.texas.gov/assets/public/implementation/air/am/contracts/reports/pm/5820784005FY1026-20100922-enviro-cb6.pdf)  
665 [0784005FY1026-20100922-enviro-cb6.pdf](https://www.tceq.texas.gov/assets/public/implementation/air/am/contracts/reports/pm/5820784005FY1026-20100922-enviro-cb6.pdf), 2010.

666



Table 1. Statistics of DM8HR O<sub>3</sub> for all model cases over the domain and analysis regions in July 2011. The best performance metrics among the model cases are highlighted in bold.

Region	Case	Record	OBS (ppb)	MOD (ppb)	RMSE (ppb)	NME (%)	MB (ppb)	NMB (%)	R
Domain	Base	36242	48.21	52.04	12.6	19.2	<b>3.8</b>	<b>8.0</b>	0.69
	mNLDN	36242	48.21	53.40	12.9	19.8	5.2	10.8	0.70
	hNLDN	36242	48.21	52.21	<b>11.9</b>	<b>18.4</b>	4.0	8.3	<b>0.72</b>
	pNLDN	36242	48.21	52.52	12.7	19.5	4.3	8.9	0.70
NE	Base	5512	50.97	55.08	13.0	17.8	4.1	8.1	0.74
	mNLDN	5512	50.97	55.77	13.4	18.5	4.8	9.4	0.74
	hNLDN	5512	50.97	54.23	<b>11.9</b>	<b>16.7</b>	<b>3.3</b>	<b>6.4</b>	<b>0.75</b>
	pNLDN	5512	50.97	55.32	13.1	18.0	4.4	8.5	0.74
SE	Base	7061	44.55	51.71	<b>12.6</b>	<b>21.0</b>	<b>7.2</b>	<b>16.1</b>	0.76
	mNLDN	7061	44.55	53.33	13.6	23.6	8.8	19.7	0.76
	hNLDN	7061	44.55	52.30	12.6	21.7	7.8	17.4	<b>0.77</b>
	pNLDN	7061	44.55	52.39	13.0	22.0	7.8	17.6	0.76
UM	Base	8072	51.60	58.99	13.6	18.8	7.4	14.3	0.64
	mNLDN	8072	51.60	60.14	14.4	20.5	8.5	16.6	0.64
	hNLDN	8072	51.60	58.35	<b>12.8</b>	<b>18.0</b>	<b>6.8</b>	<b>13.1</b>	0.64
	pNLDN	8072	51.60	59.42	13.9	19.4	7.8	15.1	0.64
LM	Base	3609	42.15	46.21	12.4	21.5	<b>4.1</b>	<b>9.6</b>	0.73
	mNLDN	3609	42.15	47.93	12.9	22.3	5.8	13.7	0.74
	hNLDN	3609	42.15	47.12	<b>12.3</b>	<b>21.3</b>	5.0	11.8	<b>0.76</b>
	pNLDN	3609	42.15	46.93	12.6	21.8	4.8	11.3	0.74
RM	Base	6256	52.52	48.13	11.3	17.0	-4.4	-8.4	0.52
	mNLDN	6256	52.52	50.93	10.2	14.7	<b>-1.6</b>	<b>-3.0</b>	0.56
	hNLDN	6256	52.52	50.35	<b>9.9</b>	<b>14.4</b>	-2.2	-4.1	<b>0.57</b>
	pNLDN	6256	52.52	48.93	10.9	16.2	-3.6	-6.9	0.53
PC	Base	5570	44.72	47.58	11.7	20.1	2.9	6.4	0.80
	mNLDN	5570	44.72	47.73	11.6	20.0	3.0	6.7	0.80
	hNLDN	5570	44.72	46.65	<b>11.3</b>	<b>19.5</b>	<b>1.9</b>	<b>4.3</b>	<b>0.81</b>
	pNLDN	5570	44.72	47.62	11.6	20.0	2.9	6.5	0.80



Table 2. Statistics of daily mean NO<sub>x</sub> for all model cases over the domain and analysis regions July 2011. The best performance metrics among the model cases are highlighted in bold.

Region	Case	Record	OBS (ppb)	MOD (ppb)	RMSE (ppb)	NME (%)	MB (ppb)	NMB (%)	R
Domain	Base	6912	7.58	8.88	<b>8.7</b>	62.6	<b>1.3</b>	17.1	0.54
	mNLDN	6912	7.58	8.87	<b>8.7</b>	<b>62.5</b>	<b>1.3</b>	<b>17.1</b>	0.54
	hNLDN	6912	7.58	8.92	8.7	62.7	1.3	17.7	<b>0.55</b>
	pNLDN	6912	7.58	8.87	<b>8.7</b>	62.5	<b>1.3</b>	17.1	0.54
NE	Base	989	10.48	9.72	<b>7.0</b>	46.0	-0.8	-7.3	0.55
	mNLDN	989	10.48	9.71	<b>7.0</b>	<b>46.0</b>	-0.8	-7.3	<b>0.55</b>
	hNLDN	989	10.48	9.77	7.1	46.1	<b>-0.7</b>	<b>-6.8</b>	0.55
	pNLDN	989	10.48	9.72	<b>7.0</b>	46.0	-0.8	-7.3	0.55
SE	Base	645	6.44	9.18	7.2	75.3	2.7	42.6	0.34
	mNLDN	645	6.44	9.17	<b>7.2</b>	<b>75.1</b>	<b>2.7</b>	<b>42.4</b>	0.34
	hNLDN	645	6.44	9.18	7.2	75.3	2.7	42.6	<b>0.34</b>
	pNLDN	645	6.44	9.17	7.2	75.2	2.7	42.5	0.34
UM	Base	542	11.42	18.09	<b>18.7</b>	<b>82.7</b>	<b>6.7</b>	<b>58.4</b>	<b>0.58</b>
	mNLDN	542	11.42	18.10	18.7	82.8	6.7	58.5	<b>0.58</b>
	hNLDN	542	11.42	18.22	18.9	83.6	6.8	59.5	<b>0.58</b>
	pNLDN	542	11.42	18.09	18.7	<b>82.7</b>	<b>6.7</b>	58.4	<b>0.58</b>
LM	Base	1240	6.11	8.32	6.0	61.2	2.2	36.1	<b>0.68</b>
	mNLDN	1240	6.11	8.30	<b>6.0</b>	<b>61.1</b>	<b>2.2</b>	<b>35.9</b>	<b>0.68</b>
	hNLDN	1240	6.11	8.33	6.0	61.3	2.2	36.3	<b>0.68</b>
	pNLDN	1240	6.11	8.31	6.0	61.2	2.2	36.0	<b>0.68</b>
RM	Base	1370	3.90	4.00	3.7	60.0	<b>0.1</b>	<b>2.4</b>	0.58
	mNLDN	1370	3.90	4.01	<b>3.7</b>	<b>59.9</b>	<b>0.1</b>	2.6	0.58
	hNLDN	1370	3.90	4.02	3.7	60.0	0.1	3.3	<b>0.58</b>
	pNLDN	1370	3.90	4.00	3.7	60.0	<b>0.1</b>	<b>2.4</b>	0.58
PC	Base	2056	8.61	9.52	<b>9.1</b>	<b>62.8</b>	<b>0.9</b>	<b>10.6</b>	0.48
	mNLDN	2056	8.61	9.52	<b>9.1</b>	<b>62.8</b>	<b>0.9</b>	<b>10.6</b>	0.48
	hNLDN	2056	8.61	9.59	9.1	62.9	1.0	11.4	<b>0.48</b>
	pNLDN	2056	8.61	9.52	<b>9.1</b>	<b>62.8</b>	<b>0.9</b>	<b>10.6</b>	0.48



Table 3. Statistics of June-August 2011 accumulated precipitation (cm) and wet deposition of nitrate (NO<sub>3</sub><sup>-</sup>) for all model cases over the domain. The best performance metrics among the model cases are highlighted in bold.

Region	Case	Record	OBS (cm, kg/ha)	MOD (cm, kg/ha)	RMSE (cm, kg/ha)	NME (%)	MB (cm, kg/ha)	NMB (%)	R
Domain	precip	196	24.8	23.9	7.5	23	-0.9	-4	0.87
	Base	196	2.34	1.52	1.1	38	-0.8	-35	0.84
	mNLDN	196	2.34	1.98	<b>0.8</b>	<b>26</b>	<b>-0.4</b>	<b>-15</b>	<b>0.86</b>
	hNLDN	196	2.34	1.95	<b>0.8</b>	<b>26</b>	<b>-0.4</b>	-17	<b>0.86</b>
	pNLDN	196	2.34	1.68	1.0	33	-0.7	-28	0.85
NE	precip	31	38.6	35.9	9.5	19	-2.7	-7	0.79
	Base	31	2.96	2.32	1.1	29	-0.6	-23	0.70
	mNLDN	31	2.96	2.71	<b>0.9</b>	<b>24</b>	-0.3	-8	<b>0.76</b>
	hNLDN	31	2.96	2.74	<b>0.9</b>	<b>24</b>	<b>-0.2</b>	<b>-7</b>	0.74
	pNLDN	31	2.96	2.48	1.0	27	-0.5	-16	0.73
SE	precip	39	36.1	31.7	9.4	21	-4.3	-12	0.80
	Base	39	3.05	2.09	1.2	35	-1.0	-32	0.51
	mNLDN	39	3.05	2.97	<b>0.8</b>	<b>21</b>	<b>-0.1</b>	<b>-2</b>	<b>0.56</b>
	hNLDN	39	3.05	2.82	0.9	23	-0.2	-8	0.53
	pNLDN	39	3.05	2.43	1.0	27	-0.6	-20	0.54
UM	precip	45	28.8	26.1	6.8	20	-2.7	-9	0.51
	Base	45	3.17	1.98	1.4	38	-1.2	-38	0.73
	mNLDN	45	3.17	2.51	<b>0.9</b>	<b>24</b>	<b>-0.7</b>	<b>-21</b>	<b>0.77</b>
	hNLDN	45	3.17	2.48	<b>0.9</b>	25	<b>-0.7</b>	-22	<b>0.77</b>
	pNLDN	45	3.17	2.15	1.2	33	-1.0	-32	0.76
LM	precip	12	12.3	10.4	4.1	29	-2.0	-16	0.90
	Base	12	1.44	0.85	0.7	41	-0.6	-41	0.90
	mNLDN	12	1.44	1.16	<b>0.6</b>	33	<b>-0.3</b>	<b>-19</b>	0.88
	hNLDN	12	1.44	1.13	<b>0.6</b>	<b>32</b>	<b>-0.3</b>	-21	<b>0.89</b>
	pNLDN	12	1.44	0.93	0.7	36	-0.5	-35	0.88
RM	precip	50	13.7	18.2	6.9	39	4.4	32	0.91
	Base	50	1.63	0.8	1.0	51	-0.8	-51	0.90
	mNLDN	50	1.63	1.1	<b>0.7</b>	34	<b>-0.5</b>	-32	<b>0.91</b>
	hNLDN	50	1.63	1.12	<b>0.7</b>	<b>33</b>	<b>-0.5</b>	<b>-31</b>	0.90
	pNLDN	50	1.63	0.86	1.0	48	-0.8	-47	<b>0.91</b>
PC	precip	19	7.01	6.53	<b>2.4</b>	29	<b>-0.48</b>	-6.8	0.84
	Base	19	0.31	0.31	<b>0.18</b>	44	<b>0.00</b>	-1.0	0.88
	mNLDN	19	0.31	0.33	0.19	48	0.01	3.9	<b>0.89</b>
	hNLDN	19	0.31	0.33	0.20	50	0.02	6.6	<b>0.89</b>
	pNLDN	19	0.31	0.31	<b>0.18</b>	44	<b>0.00</b>	<b>-0.3</b>	0.88

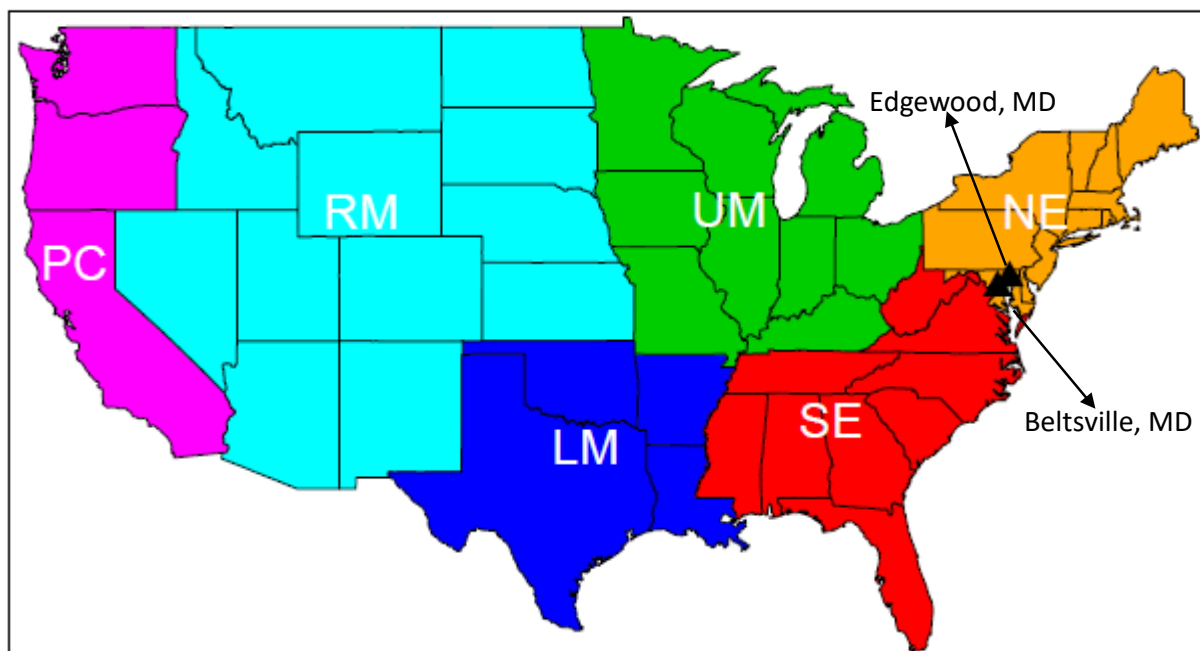


Figure 1. Analysis regions and ozonesonde locations during the 2011 DISCOVER-AQ field study.



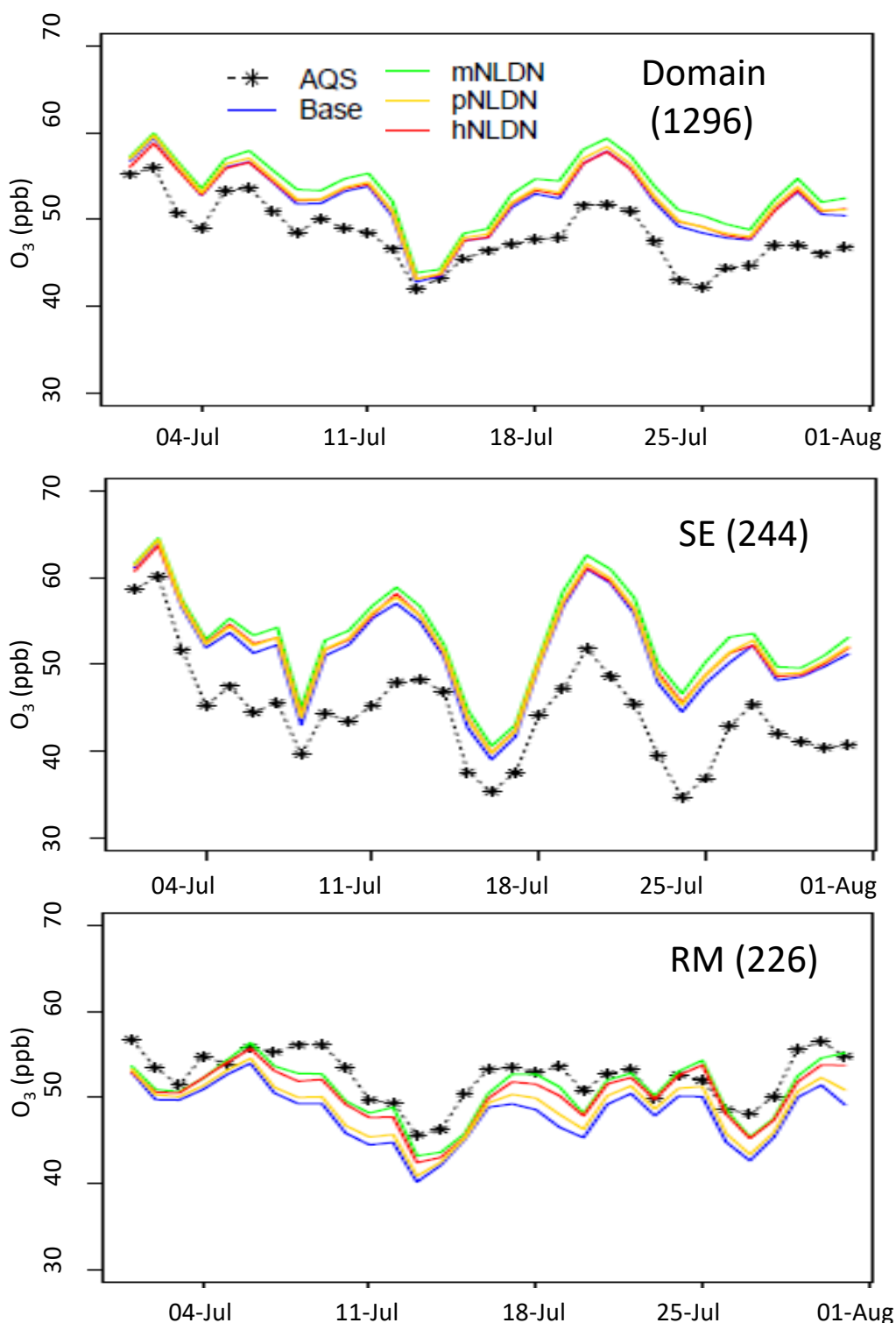


Figure 2. Timeseries of regional-mean daily maximum 8-hr  $O_3$  comparing observations (AQS) and CMAQ model predictions using the  $LNO_x$  schemes to Base simulation for the domain (a), SE (b), and RM (c) in July, 2011. The numbers in the parentheses following the region names are the number of AQS sites.

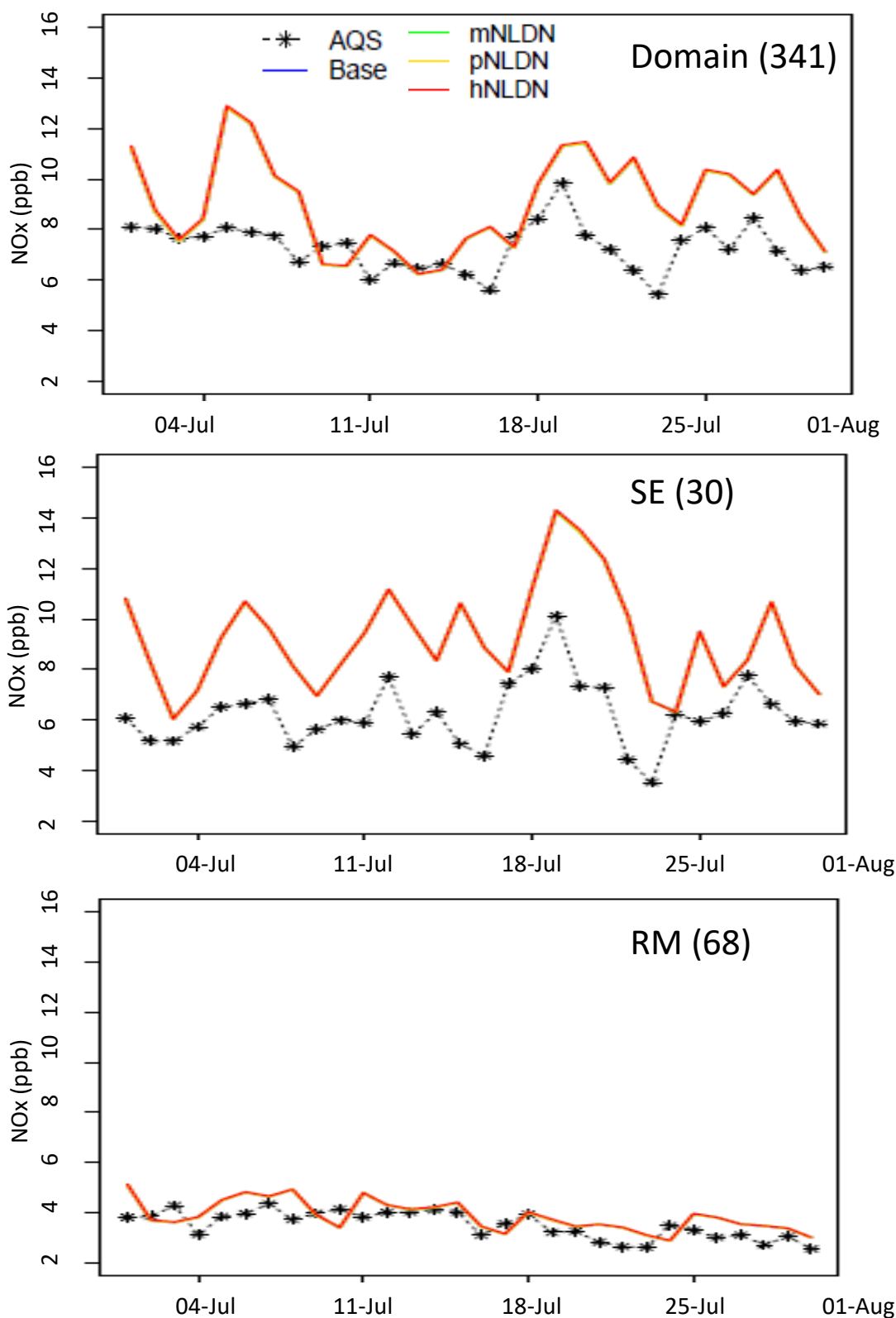


Figure 3. Timeseries of daily mean NO<sub>x</sub> over the domain (a), SE (b), and RM (c) in July, 2011. The numbers in the parentheses following the region names are the number of AQS sites.

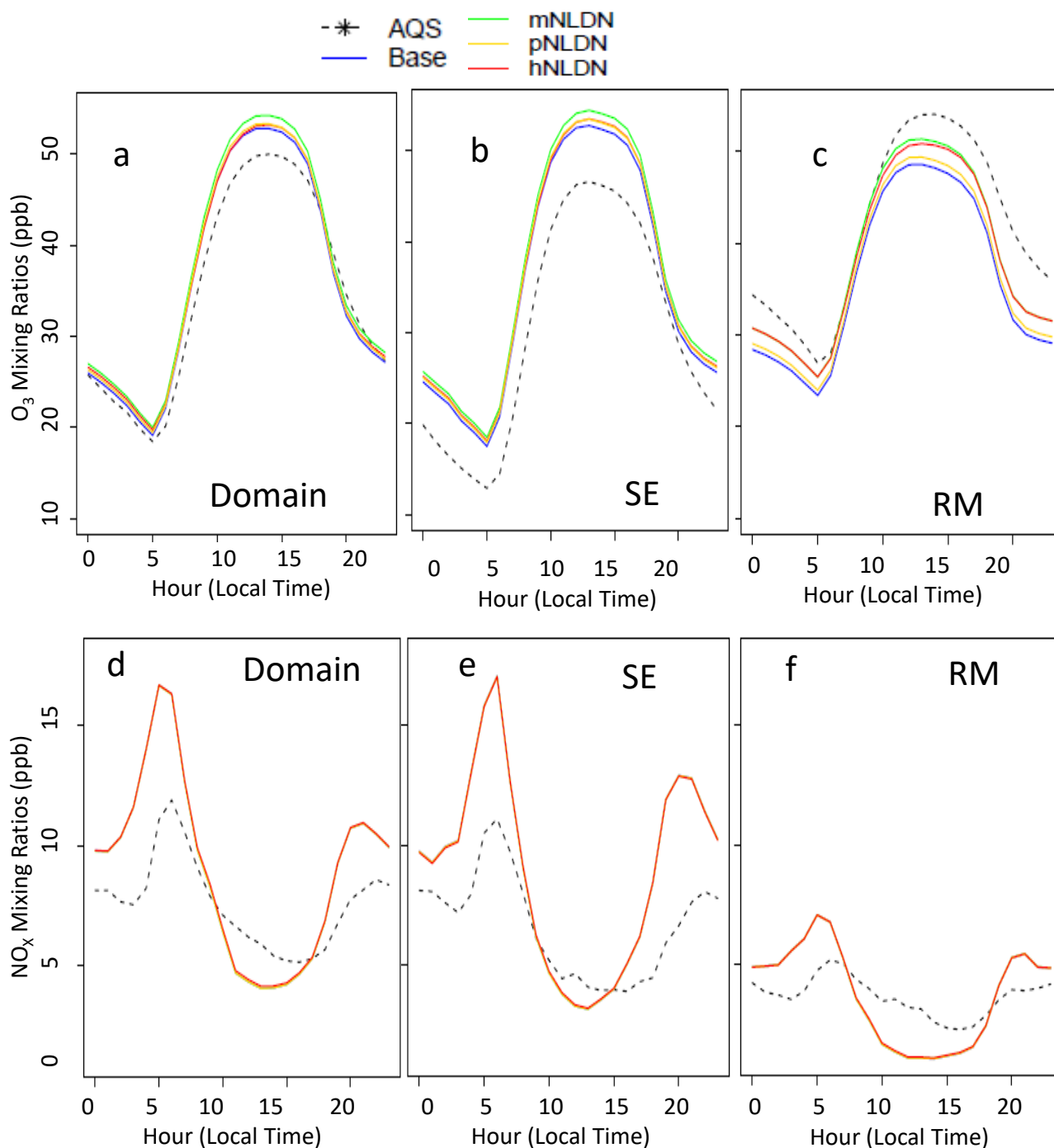


Figure 4. Diurnal profiles for hourly  $O_3$  and  $NO_x$  over the domain (a,d), SE (b,e), and RM (c,f) in July, 2011.

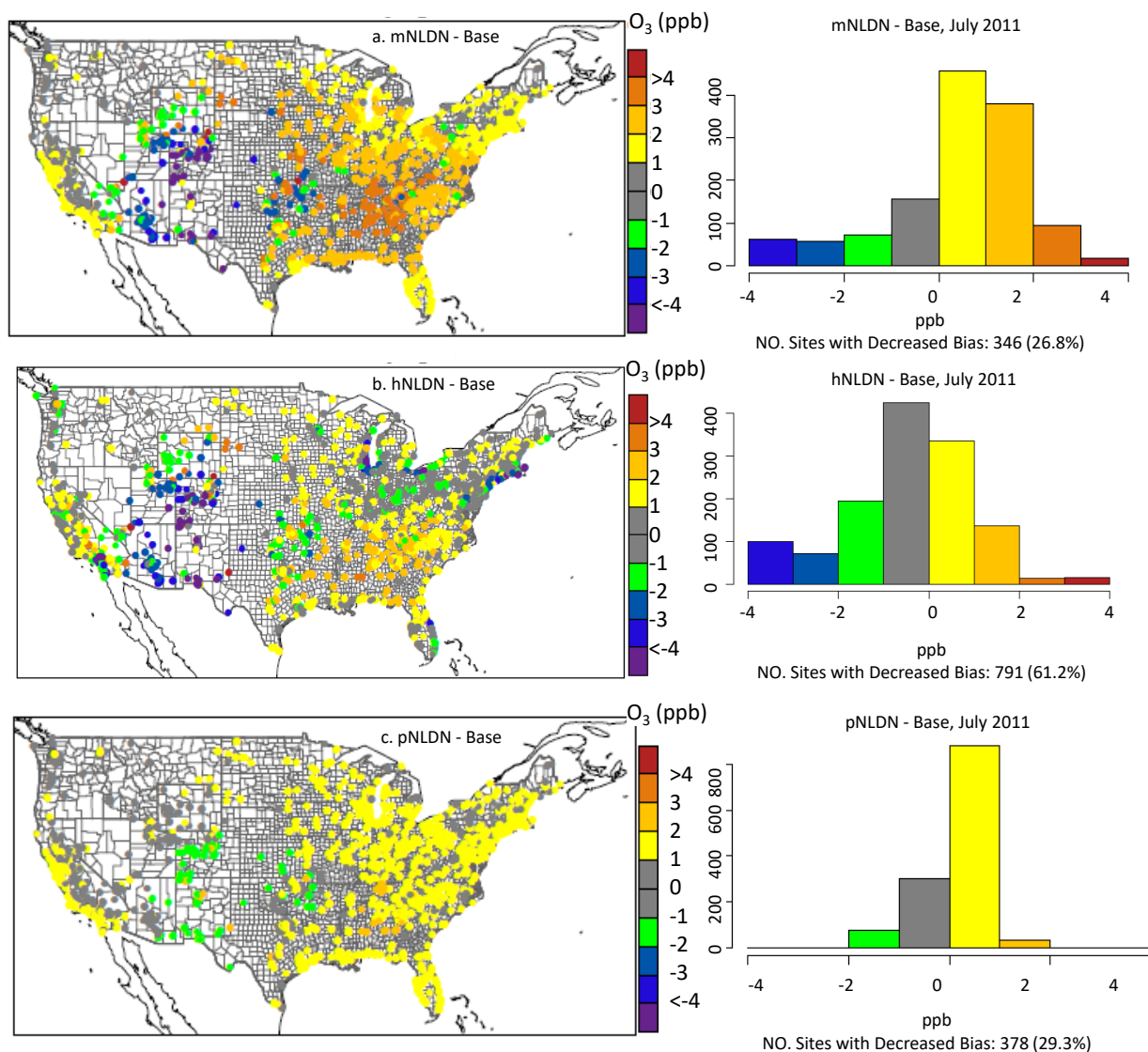


Figure 5. Spatial maps of the mean bias of DM8HR O<sub>3</sub> (model – observation) differences between model case with LNO<sub>x</sub> and the Base as well as the corresponding histograms indicating the number of sites with decreased mean bias for each pair of model cases in July, 2011.

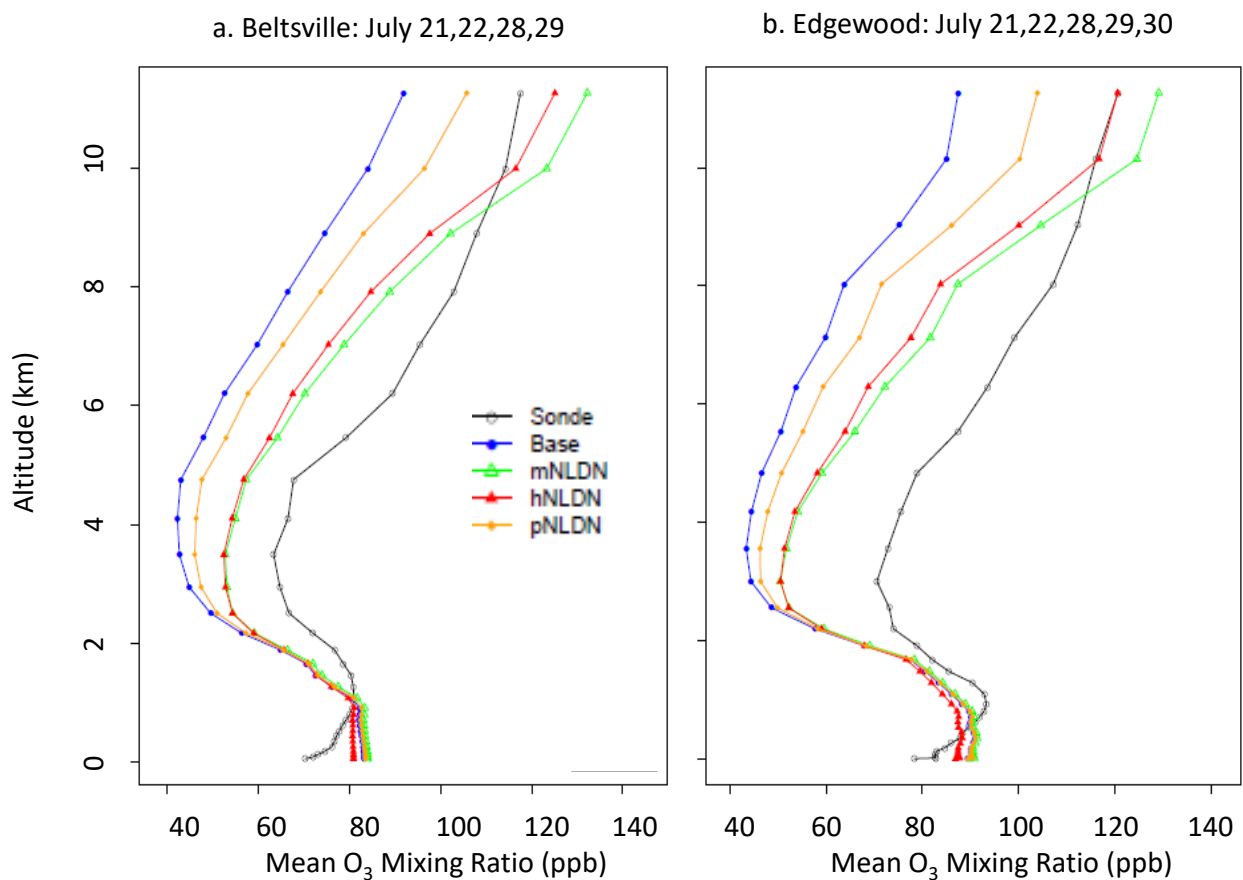


Figure 6. Vertical profiles of O<sub>3</sub> mixing ratios from ozonesonde measurements and model simulations at Beltsville, MD (a) and Edgewood, MD (b) on the days when lightning NO produced significant impact on O<sub>3</sub> during the Discover-AQ field study in July, 2011.

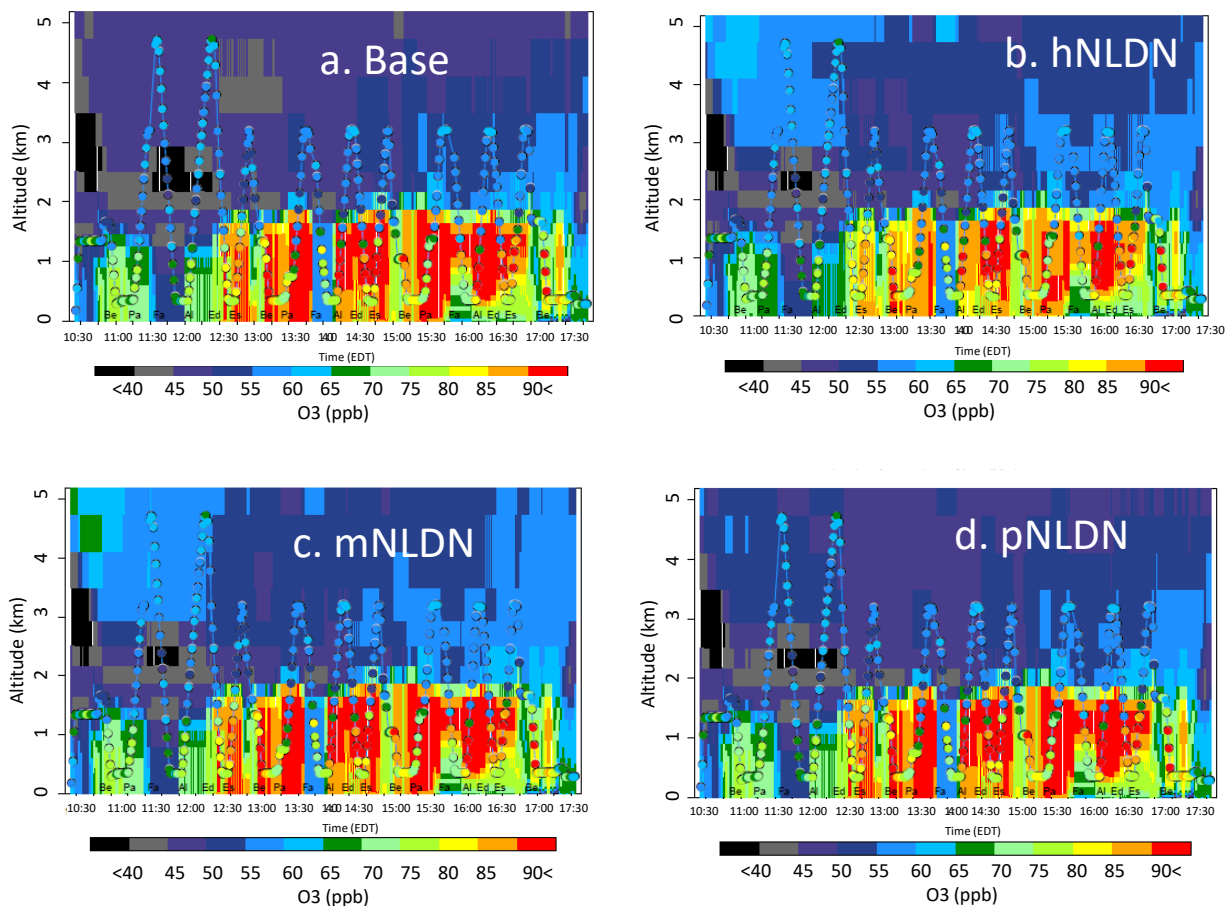


Figure 7. Overlay of P3B observed O<sub>3</sub> (1 minute mean values) over the corresponding vertical cross sections of simulated values extracted at the flying locations on July 28, 2018, (a) Base, (b) hNLDN, (c) mNLDN, and (d) pNLDN. The letters marked at the bottom of the plots are P3B spiral sites, Be: Beltsville, Pa: Padonia, Fa: Fairhill, Al: Aldino, Ed: Edgewood, Es: Essex.

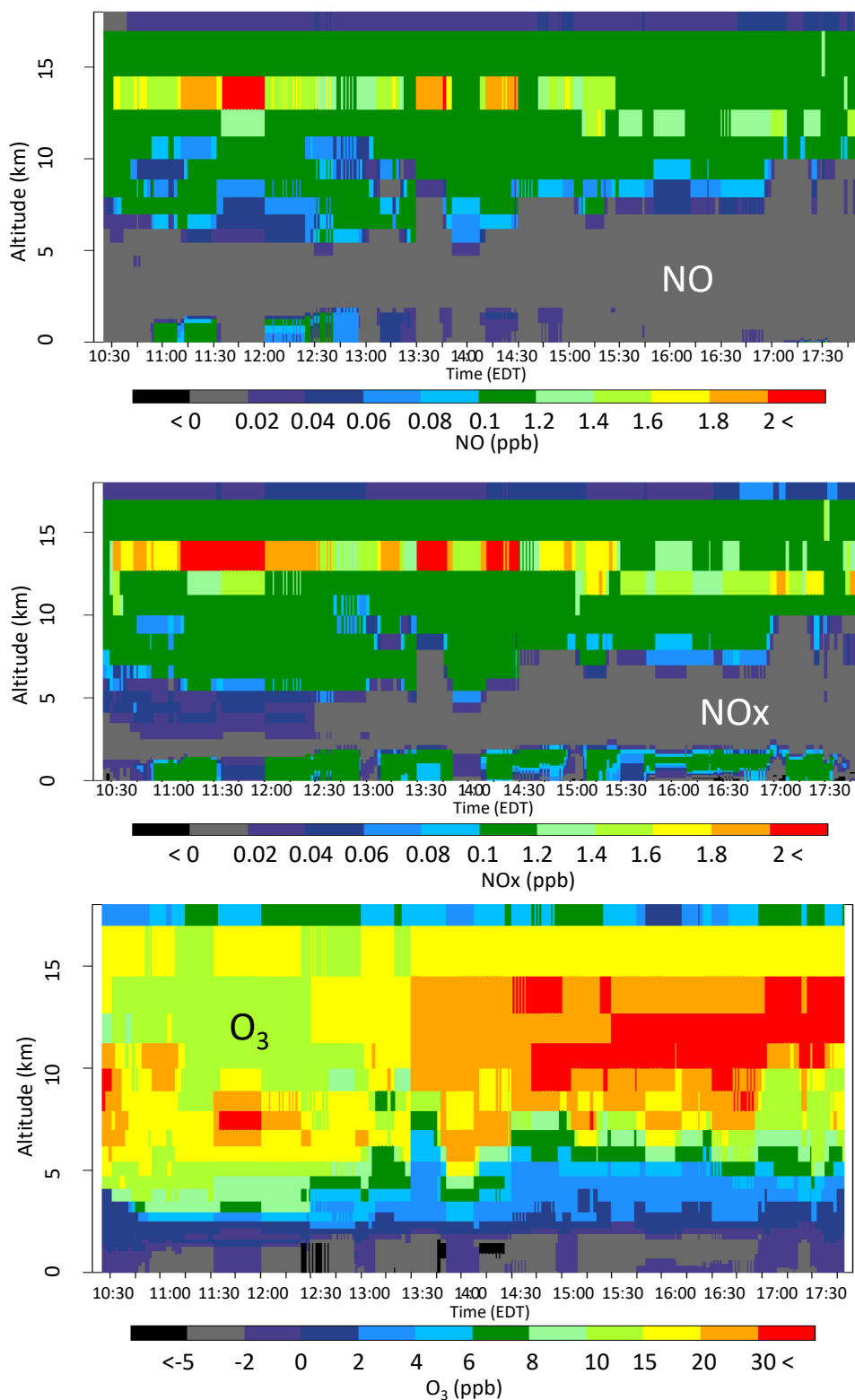


Figure 8. The vertical-time difference between hNLDN and Base during the P3B flight period on July 28, 2011 for (a) NO, (b) NO<sub>x</sub>, and (c) O<sub>3</sub>.

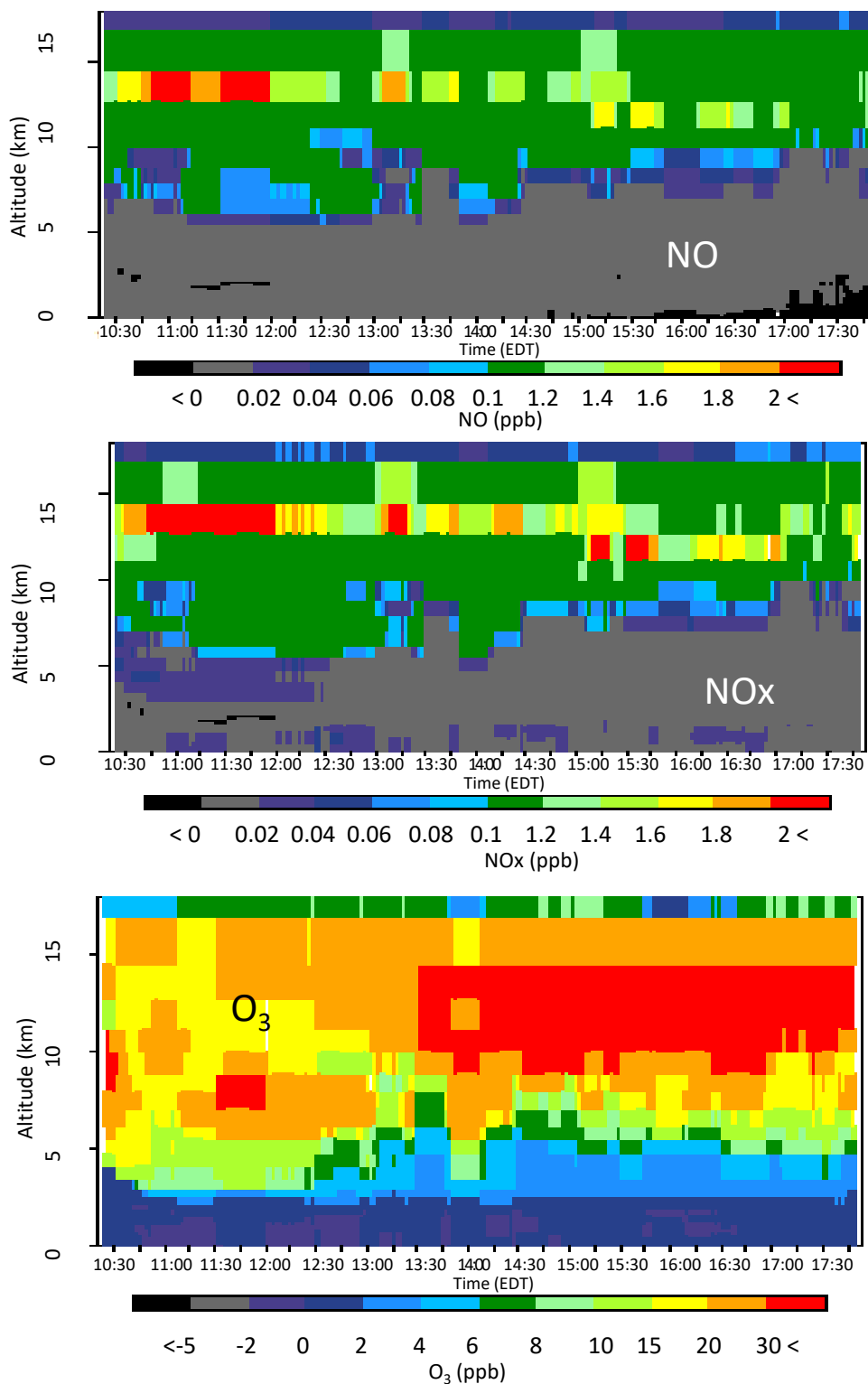


Figure 9. The vertical-time difference between mNLDN and Base during the P3B flight period on July 28, 2011 for (a) NO, (b) NO<sub>x</sub>, and (c) O<sub>3</sub>.



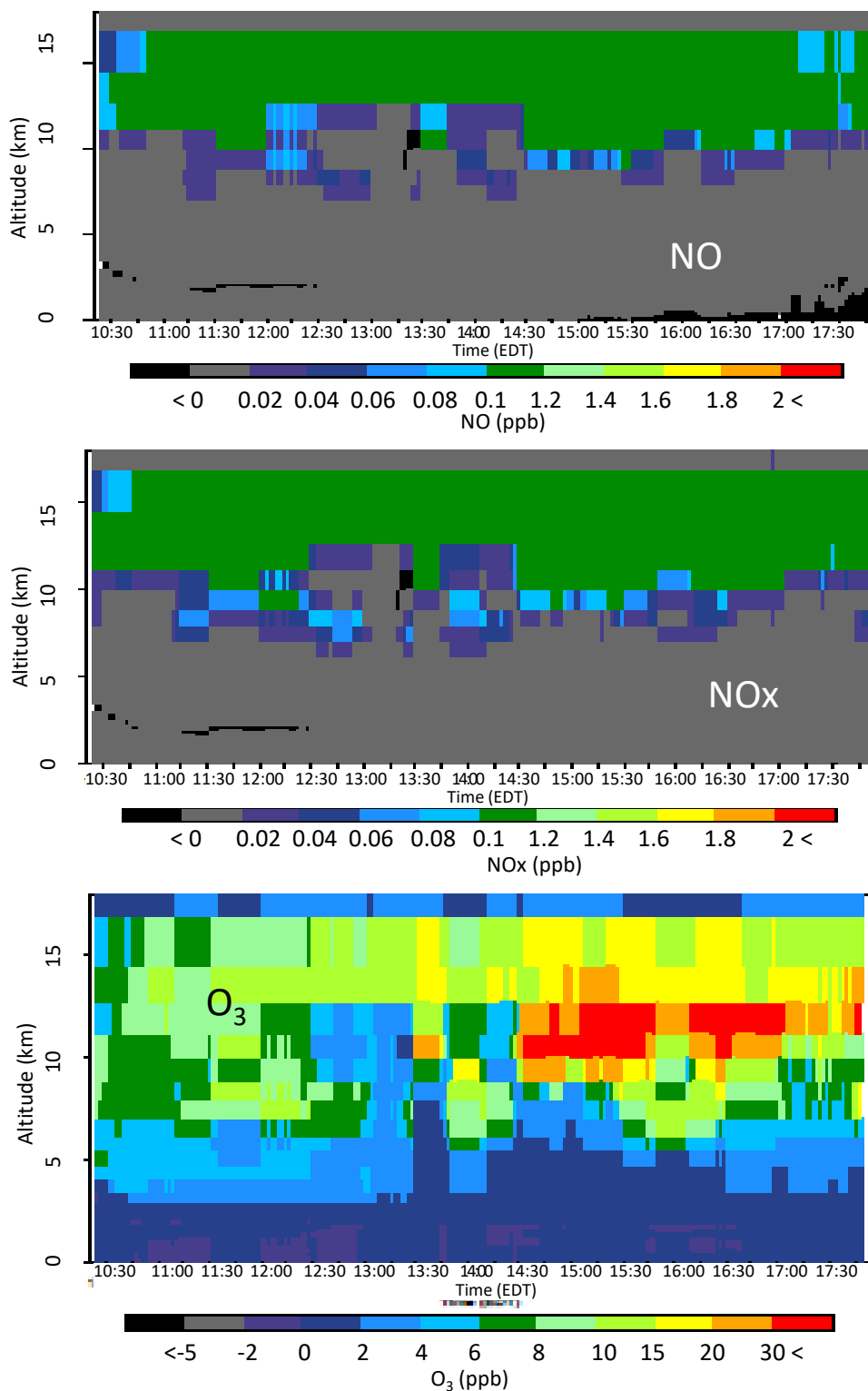


Figure 10. The vertical-time difference between pNLDN and Base during the P3B flight period on July 28, 2011 for (a) NO, (b) NO<sub>x</sub>, and (c) O<sub>3</sub>.

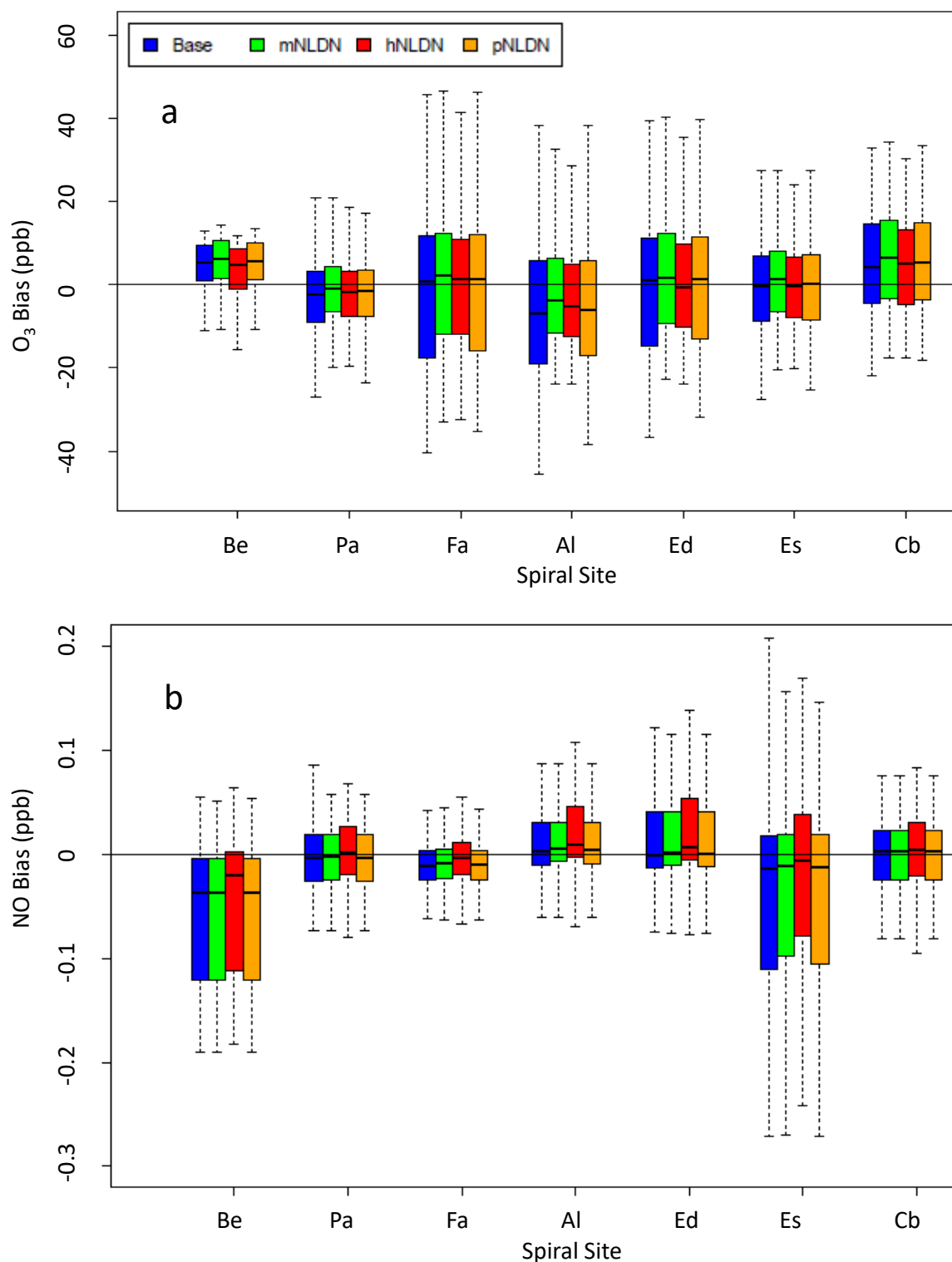


Figure 11. Bias (model – observation) distributions of O<sub>3</sub> (a) and NO (b) at each P3B spiral site on July 21, 22, 28, and 29, 2011. Be: Beltsville, Pa: Padonia, Fa: Fairhill, Al: Aldino, Ed: Edgewood, Es: Essex, Cb: Chesapeake Bay.

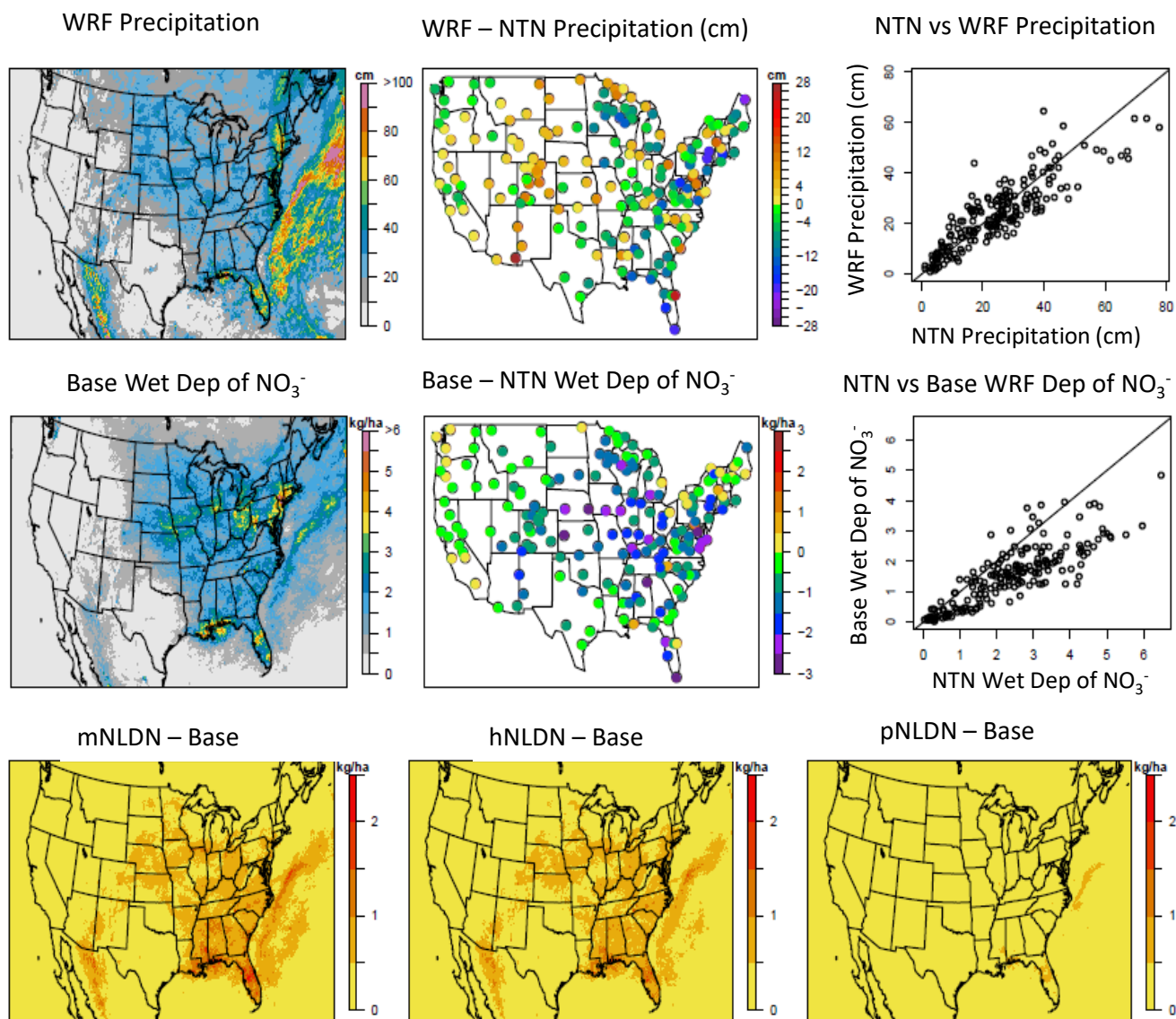


Figure 12. The top row shows precipitation estimates from WRF (left), the bias in the WRF predicted precipitation at NTN locations (middle), and the corresponding scatter plots (right). The middle row shows wet deposition (Dep) of nitrate estimates from the Base simulation (left), the bias in the Base model estimates of wet deposition of  $\text{NO}_3^-$  at NADP/NTN locations (middle), and the corresponding scatter plots (right). The bottom row shows the difference in the LNO<sub>x</sub> sensitivity simulations and the Base case estimates of wet deposition of  $\text{NO}_3^-$ : mNLDN - Base (left); hNLDN - Base (middle), and pNLDN - Base (right). All maps are based on accumulated values (precipitation or wet deposition) during June - August 2011. Precipitation totals are in cm and wet deposition totals are in kg/ha.